DYNAMICS OF PLANKTON POPULATIONS IN UPWELLING AREAS

Karl-Heinz Szekielda

University of Delaware

Contract Number: NAS5-21784

June and July 1973

The continued investigations to use ERTS-1 recordings for plankton studies showed the following identified features:

1. The distribution of plankton in upwelling areas is much more complicated than indicated by conventional methods aboard ships.

2. Fast changes in horizontal plankton concentration appear.

3. Wind stress seems to be the important factor in controlling the patchiness and disappearance of high plankton concentration.

The satellite studies over our testsite were summarized during an upwelling symposium at Marseille. A tentative manuscript which will be part of the final report to NASA in attached.

1. INTRODUCTION

The operation of an orbiting system at high altitudes limits the ground resolution as well as the signal to noise ratio. Therefore, with the recent technology, satellites are especially an advantage in areas with high horizontal temperature and color gradients. Upwelling areas are the most promising regions for an application of remotely sensed data from space (Szekielda, 1972).

By using multispectral methods (Shenk and Salomonson, 1972) the most interferring factors, namely water vapours and clouds, can be eliminated. Also statistical methods for cloud elimination show a promising potential to use satellite information for oceanographic purposes (Smith, Rao, Koeffler, and Curtis, 1970; LaViolette and Chabot, 1969).

The recent plans to investigate the upwelling area along the NW Coast of Africa include studies with satellites. The detection of patchiness in temperature and plankton distribution in the upwelling area along the NW Coast of Africa is of special interest because they can be investigated from space on a synoptic way with repeated coverage.

The recent satellite missions provide recordings in the infrared region of the electromagnetic spectrum (EMR) as well as in the visible part. The information from those two parts of the EMR is useful for establishing the sea surface temperature and plankton distribution in upwelling areas. In this paper one part deals with the temperature

distribution as observed with infrared sensors and the second part will discuss the patchiness in plankton patterns as observed with the most recent satellites, namely the Earth Resources Technology Satellite (ERTS) and NOAA-2.

2. ATMOSPHERIC CONDITIONS AND WIND SYSTEMS

Although research is underway to eliminate atmospheric attenuation of electromagnetic energy from a test site, careful examination of atmospheric influences on the final results have to be considered.

The climate along the West Coast of Africa between the Strait of Gibraltar and the Cape des Palmes is determined by two anticyclonic systems near the Azores. Atmospheric attenuation is low for Morocco, Spanish Sahara, Manritania, Senegal, Portuguese Guinea, Guinea, Sierra Leone and Liberia. Abnormal conditions like sandstorms, which transport fine sand particles and dust over great distances, winds from the continent and also the building of fog over the near coastal cold water during the morning to afternoon, may change the visibility for shorter periods. Since the anticyclonic system of the Azores exists with its high pressure throughout the entire year, changes in the atmospheric conditions are only small. During winter time of the northern hemisphere, the high pressure system with 1012 mb is centered between the Canary Islands and the Azores and continuous to the east to Morocco. Toward the South the pressure reduces toward the Intertropical Convergence Zone.

During the summertime the anticyclonic system extends to the North and the West with an increase in pressure of 1026 mb in its center at about 35°N and 45°W. This can be recognized in the normal daily weather charts. The wind regimes can be qualitatively divided into a zone of variable winds in the North, the area of the Northeast winds (called Alize de NE in

French), the Intertropical Convergence with calm winds in the equatorial region, and the Alize in the South with a Southeast component. As a result, the cloud coverage as viewed from space reflects also the different wind systems. Fig. 1 shows the cloud coverage in the near equatorial region as part of the ITC.

The Alize NE is of most importance for the upwelling conditions near the NW Coast of Africa. Its deplacement as well as its strength is a function of the position of the anticyclone. Normally the Alize NE covers during winter the area between 5°N and 30°N and during summer the area between 15°N and 35°N. The wind force is between 3 and 4 Beauforts.

In the region of the Alize NE, nice weather is very common with an extremely good horizontal and vertical visibility. For satellite studies this area gives a good opportunity to study surface structures in the water as well as geological and biological (vegetation) features in the coastal zone. Fig. 2 is an example where the low albedo levels as obtained with a television camera indicate cloudfree conditions.

The ITC in the zone of calm equatorial winds is situated between the Alize NE and the Alize SE. In February it covers the meridian 100 miles and in August 300 miles. The ITC is an outstanding feature in satellite imageries and is visible in the infrared as well as in the visible spectral region.

South of 15°N the NE winds are especially a result of the valley of continental depression and termed Harmattan. These winds are less frequent

in the area around Mauritania but well developed in the South. They are frequent from November through February and seldom in March-April. At higher altitudes they exist during the entire year and overlay the Alize, or north of Dakar it may be placed over the monsoon. The Harmattan has its origin in the desert regions on the continent and is characterized by a dry atmosphere, which favors observations from space to investigate surface features of the oceans. Aperiodically the Harmattan is charged with dust which influences the horizontal and vertical visibility but only for short times. The Harmattan reaches the ground only during the monsoon period. At this time the atmospheric fallout should reach its maximum. The intensity of the Harmattan is sometimes reduced and reaches an equilibrium between the seabreeze at lower altitudes, or is completely diminished.

Near the Canary Islands the dominant winds are from North to NE. In November through January the Alize is sometimes replaced by winds with a south and/or west component. As a function of the extension to the South and East, the anticyclone of the Azores transports warm and dry winds from the South to the Island Tenerife. An almost transparent atmosphere with a small amount of aerosols is the result and the Canary Islands are easily detectable by sensors working in the thermal infrared and in the solar reflected energy. The pictorial display of data monitored in the visible part of the electromagnetic spectrum shows the islands very sharply (Figs. 3 and 4). Madeira also is still influenced by the same meteorological system, but the wind direction may be E or ESE (called Este at Madeira). This area might be the northern limit to obtain good coverage from space with a single orbit, but with repeated coverage of this area cloudfree orbits may

be obtained. Near the Canary Islands the inverse movement of the seabreeze may create a calm zone in the near coastal area of the islands.

The Alize NE is dominant the entire year in the region of the Cape Verde Islands. During December, January, and February the Harmattan is very frequent with fine dust but is replaced during the rain period from August through October by winds from the South.

Along the Coast of Morocco in the north, two major directions of the winds are dominant: (1) The "Levantes" which is a dry strong wind with a Northeast to East component and (2) the "Ponientes" which is also strong but humid with a velocity of 45 to 60 knots. To the west, the Alize NE may change its direction during summer to Northwest as a function of the seabreeze. Under normal weather conditions the maximum wind speed may be in the afternoon. The competition between the seabreeze and the Alize also may influence the visibility.

When the Alize goes further south during winter, the north and northeast winds are still frequent but interrupted by winds with a southwest component. At the end of the summer a hot wind (Sirocco or locally called Chergu) has a south or southeast direction and transports dry air commonly loaded with sand.

More to the South at Agadir, the wind direction is modified since the winds from east and west are present with the same egality.

The Alize with a north or northeast direction respectively are predominant the entire year along the Coast of Spanish Sahara and Mauritanai.

The north component is more pronounced in summer while the east direction dominates during wintertime. This is shown in the wind field as given in Fig. 5. The seabreeze is well developed to about 20-30 miles from the shore.

The low frequency of cloud appearance along the NW Coast of Africa can be demonstrated with albedo measurements obtained with the Medium Resolution Infrared Radiometer (MRIR) on Nimbus III. One channel of this instrument recorded the outgoing radiation between 0.2 to 4.0 μm and covered more than 99% of the solar reflected energy. All collected measurements from this channel were averaged over a period of two weeks.

The effective mean radiance over this period of time is shown in Fig. 6 where the radiant reflectance $\bar{r}$ is normalized by

$$\bar{r} = \frac{\pi \bar{N}}{\overline{H^*} \cos\sigma^*}.$$

$\overline{H^*}$ is the integral over all wavelength of the solar spectral irradiance at the top of the atmosphere multiplied by the effective spectral response, $\bar{N}$ the effective radiance and σ^* the solar zenith angle.

The analysis of Fig. 6 shows the NW Coast of Africa between 11°N and 35°N where the sharp gradient represents the interface between the continent and the water. High albedo on the right hand side indicates the Sahara Desert.

The frequency distribution of the data showed an albedo for water viewed under cloudfree conditions of less than 8. Albedo less than 10

between 23°N and 11°N shows that clouds are rarely found between Cape Blanc and Cape Verde within a 14 day period. Above 30°N more frequent cloud coverage is indicated by increasing albedo toward the north.

3. TEMPERATURE OBSERVATIONS

The recent studies include the analysis of data which were collected during different spacecraft missions. Mainly, the data from scanning radiometers in the infrared and television cameras for the visible were applied to derive temperature data over cloudfree regions.

The purpose of the first part of this paper is to give a qualitative estimate of possible variations in sea surface temperature in the upwelling area along the NW Coast of Africa. The importance of such investigation is demonstrated by the presence of very complicated surface structures of temperature, nutrients, and chlorophyll in the upwelling region (Weichert, 1970; Ballester, Cruzado, Julia, Manriquez, and Salat, 1972).

The fast response of surface temperature to changes of the wind field were observed for the first time with the Nimbus II and III satellites in the upwelling region along the Somali Coast. Düing and Szekielda (1971) made a statistical comparison between the wind speed and the development of horizontal temperature gradients. As a result it was concluded that the response time of the development of surface temperature gradients onto the wind stress is in the order of 2-4 days, which is a surprisingly fast response of the vertical transport onto the wind. Unfortunately, almost no data are available to estimate the surface temperature changes as a function of the wind systems along the NW Coast of Africa.

Temperature patterns in the test site along the NW Coast of Africa were detected with the Temperature Humidity Infrared Radiometer (THIR)

from the Nimbus IV satellite. A period between 18 April and 6 May, 1970, was selected when noise level of the instrument was low. Also the cloud coverage showed a minimum at this time, which resulted in a repeated coverage for the temperature in the upwelling area. Temperature was recorded in the atmospheric window channel at 10.5 μm to 12.5 μm. The ground resolution at the subpoint was eight kilometers from an altitude of 600 nautical miles. The water vapor channel at 6.7 μm was also used to give qualitative information about the moisture content of the upper troposphere and stratosphere as well as the location of jet streams and frontal systems.

Cloudfree conditions were detected with the Image Dissector Camera System (IDCS) flown on the same satellite. The daytime pictures were taken simultaneously when THIR recorded temperature patterns.

A complete timing cycle of one frame needed 208 seconds (Werner and Branchflower, 1970) and consisted of 800 scan lines per one entire image dissector video frame. Since a minus blue filter in front of the lens was employed, the detection of clouds is strongly enhanced.

The ground resolution from the IDCS was approximately two nautical miles at the nadir with a decrease to five nautical miles near the edges of the field of view. That means consequently that the IDCS in connection with the THIR is a good qualitative indication of whether a structure in the infrared data is produced by the sea surface temperature or by cloud features.

The area covered in the following analysis lies between the Canary

Islands at 28°N and Cape Verde (Dakar) at 15°N. Typical samples of the original black and white infrared image and the television picture is displayed in Figs. 1 and 2. The color enhancement was made from the black and white pictorial display of the IDCS and THIR with a density slicing machine where gray levels were displayed in color on a television screen. The color scale, black-purple-orange-yellow-green-blue-white showed the black body temperature from warm (black) to cold (white). The low albedo was enhanced to be black in the television image and high albedo was displayed in white.

Fig. 7 shows the IDCS picture and the infrared image from April 18, 1970. Extremely low albedo was measured along the coast of NW Africa as indicated by the dark area. Rio de Oro is visible by the coastal region displayed in blue, green, and yellow. Slight gradient in the albedo was measured offshore as indicated from the color change purple to yellow. However, no sharp gradients are visible in the albedo which indicates cloudfree conditions.

The corresponding infrared image shows the continent and islands in black according to their high black body temperature during the daytime. From the Canary Islands Lanzarote, Gran Canaria, Tenerife, and Gomera are visible. In the southern portion of the display San Antão and São Vicente are visible as part of the Cape Verde Islands.

The structure in the distribution of the infrared data and the albedo level as detected with the camera system show that slight cloud contamination occurs only in the small portion of the northern part of the recordings.

That means that the meandering and patchiness as shown in the infrared data is a surface feature. From earlier experiments (Szekielda and Mitchell, 1972) we established that each color step in the enhancement corresponds to approximately two centigrades. Therefore, a temperature gradient in the surface water of about eight degrees appears through the horizontal plane of the enhanced imagery.

On April 20, 1970, cloudfree conditions were detected with the IDCS between 8°N and 24°N (Fig. 8). According to the albedo measurements the region close to Cape Blanc shows an extremely dry and cloudfree atmosphere. Toward Cape Verde an increase of aerosols is indicated by the increased albedo levels. Small portions over the continent are cloud contaminated. They are displayed as a light blue pattern. The corresponding enhanced image from the black body temperature recordings with THIR showed the coldest water in green. The analysis indicated that upwelled water is limited to a very narrow band parallel to the coast. It covered the area between 25°N and 16°N and had a width of about thirty miles. The high radiation at about 11°N (as displayed in dark red) shows the southern limit of cold surface water.

According to the geostrophic circulation (Fedoseev, 1970) a cyclonic gyral with the center to the South Coast of Cape Blanc is a permanent feature. For the spring season considerable eddy formation has been reported, especially south of Cape Blanc. This is not reflected in the surface radiation on 20 April because only high temperatures were recorded in the South.

On April 22, 1970, the image obtained with the IDCS again indicated cloudfree conditions between 25°N and 14°N along the NW Coast of Africa (Fig. 9). The corresponding enhanced infrared image shows that the structure in surface temperature patterns changed drastically if compared to previous recordings. Relative warmer black body temperatures were measured in the north as indicated by the dark and purple colors over the ocean. The building of separated cold water patches (enhanced in greenish-blue) indicated a starting change in the surface parameters.

A similar analysis was made April 25, 1970, with the IDCS and THIR (Fig. 10). The infrared data show a patchiness in temperature with two cold centers between Cape Blanc and Cape Verde. Near coastal areas had relatively warmer temperatures.

This situation is in agreement with the geostrophic circulation of surface waters as reported by Fedoseev (1970). In April the Canary Current has normally a decreased intensity, and turns at about 25°N to the African Coast into a cyclonic water movement. The center of another cyclonic gyre has its position at about 20°N and could explain the separated colder water mass found with THIR. Tomczak (1970) reported data on temperature variations of maximal 1.4°C in the upper 30 meters. In near surface waters the changes are expected to be higher.

The fast changes in remotely sensed sea surface temperature as observed over a four day period does not mean necessarily that the main circulation changed completely. But we can conclude from this observation that other surface features might also change very quickly. This has to be considered if biological and chemical parameters in the surface waters are discussed. This especially is important if only discrete sampling is

applied in upwelling regions.

Fast changes in surface temperatures can be best detected in near coastal areas with high horizontal temperature gradients. Recent analysis of remotely sensed temperature data indicated that also offshore regions undergo a fast change in respect to surface temperature, although the change is less pronounced.

Weekly mapping of sea surface temperature between 15°N and 30°W and 10°N and 30°N is underway with NOAA-2. The method is based on a data collection over one degree squares and in using a statistical approach to determine the blackbody temperature over cloudfree areas. Fig. 11 shows a digital printout from 26 April 1973. Asterisks are identifying the coastline. Some indication of the presence of the Canary Current is given by the deformation of the isotherms in northeasterly direction. The temperature analysis of May 3, 1973, showed a slight cooling in the near coastal area. This is best indicated by comparing the position of the 22°C isoline in Fig. 11 and Fig. 12. The thermal radiation from a blackbody radiates mainly from the first microns at the surface. Since evaporation takes place at the ocean's surface, the blackbody temperature of water is somewhat lower than the actual sea surface temperature. This is due to the fact that energy is used to transfer liquid water molecules through the interface to the gas phase. However, the "cool film" at the air-sea interface shows only tenths of a degree deviations from the actual temperature. The temperature changes as found in our analysis indicate rather different vertical mixing intensities due to changes in wind stress.

4. OBSERVATIONS IN THE VISIBLE PART OF THE ELECTROMAGNETIC SPECTRUM

The radiation from the ocean's surface as measured with an orbiting photometer or spectrometer is primarily a result of incident radiation specularly reflected from below the air-sea interface and the upwelling radiation. Curran (1973) modelled the atmospheric influence on color ratios remotely sensed from space.

The radiance upwelled from the water column is a function of particles and/or sediments as well as organisms in the water and dissolved colored organic compounds like, for instance, humic acids and pigments in the cells of phytoplankton. If the sunglint has been avoided, the albedo $A_s(\lambda)$ of the ocean's surface may be described by the wavelength dependent radiance $I(\lambda)$, the irradiance incident on the ocean surface from above.

$$A_s(\lambda) = \frac{\pi I(\lambda)}{F_s(\lambda)}$$

The irradiance $F_s(\lambda)$ is a composite of directly transmitted solar irradiance and the diffuse radiation. The most simple description of the two components can be given by

$$F_s(\lambda) = \mu o F_t(\lambda) + F_D(\lambda)$$

where $F_s(\lambda)$ represents the irradiance, $\mu o F_t(\lambda)$ is the directly transmitted solar energy; μo is the cosine of the solar zenith angle. $F_D(\lambda)$ is the diffuse incident part of the incoming radiation from space.

Any outgoing radiation from the ocean surface will be influenced by

aerosols and molecular constituents. Curran (1972) used for an atmospheric transfer model the optical depth $\Gamma(\lambda)$ which is defined by

$$\Gamma(\lambda) = \int_0^\infty n\ (z)\ \beta_A\ (\ ,z)\ dz.$$

This integration is over altitude z. n(z) is the particle number density and β_A (,z) the volume scattering coefficient.

The number density dn (z,r) was based on an assumed power law distribution with size parameter v*, the particle radius r in micrometers, and altitude z in kilometers.

$$dn\ (z,r) = c(z)\ r^{-(v^* + 1)}\ dr$$

The aerosol optical depth is wavelength dependent. Since Clark, Ewing and Lorenzen (1970) used color ratios, Curran calculated wavelength dependent properties for different values of v* and came to the conclusion that the optical depth must be known to an accuracy of ± 0.01 which makes precise vertical measurements necessary. However, if one assumes that the horizontal values for the aerosol optical density are constant over a certain distance interval, useful information about the position and the strength of plankton gradients from space can be obtained.

The albedo measured at satellite altitudes differs from the measured radiance obtained at a surface level in respect to the total irradiance incident at this level. The albedo Ag(λ) measured with a satellite is defined by

$$Ag(\lambda) = \frac{\pi I(\lambda)}{\mu_o Fo(\lambda)}.$$

$Ag(\lambda)$ is termed the geometric albedo, in order to distinguish between the satellite measured albedo and the albedo defined in equation (2). $\pi I(\lambda)$ is the nadir radiance, μ_o the cosine of the solar zenith angle and $Fo(\lambda)$ is the wavelength dependent solar irradiance at the top of the atmosphere.

The most possible accuracy calculated with the model by Curran (1973) showed that useful measurements can be made from satellite altitudes to estimate the chlorophyll concentration. This statement is true especially for strong gradients of plankton in upwelling areas where concentrations of chlorophyll higher than one microgram per liter with maxima up to 40 $\mu g \cdot l^{-1}$ and more can be found.

In respect to monitoring plankton or biomass from high altitudes we have to consider the fact that algae behave rather like a suspension than a pure solution of chlorophyll. That means that solar light will be scattered at the outer shell of the plankton organisms. The absorption of incident irradiance by the cells depends on its outer structure and the optical density of the cell inside. Variations in optical density or the configuration of the cells may change the intensity of backscattered light even if the incident solar irradiance, sun angle, and the chlorophyll concentration per unit of volume remain constant. Yentsch (1960) found that the red absorption band of chlorophyll has little influence on water color. That means that the signal obtained with an orbiting spectrometer would record primarily the effect of backscattered light from the organisms.

The intensity of backscattered light caused by plankton from the ocean as a function of wavelength is given in Fig. 13. Gulf Stream water was used as a reference water assuming that the chlorophyll concentration

of less than 0.05 $\mu g \cdot l^{-1}$ does not change significantly the backscattered light compared to pure water. Assumptions were made for the interpretation of the different spectra that sky conditions, sun angle, and sea state were the same over both sites. The spectrum in Fig. 13 is the difference in energy between the spectrum obtained in near coastal water and the spectrum recorded over the Gulf Stream.

If both water masses would have had the same optical characteristics, the energy difference in both spectra should be equal to zero. That means that any differences between the two signals are caused by dissolved and/or particulate matter in the sea. If chlorophyll would effect the backscattered light by its absorption properties, we might expect differences near the absorption bands of chlorophyll.

Chlorophylls have two main absorption maxima in the visible region of the electromagnetic spectrum. The main absorption peaks for pure chlorophyll-a are at 0.446 μm and 0.663 μm. However, the naturally occurring chlorophyll-a types in plants have spectra with peaks near 0.673 and 0.683 μm. Other forms show maxima near 0.690 and 0.710 μm.

Fig. 13 is some indication for the first and second absorption maximum which appears at 0.66 μm. But the maximum of backscattered light appears at 0.58 μm. Considering only the portion from the maximum toward the near infrared, it is obvious that beside small changes, decrease of the backscattered light appears. This is some indication that beside the absorption of light by chlorophyll, backscattered light from the organisms themselves contributes to the total backscattered energy. Thus, the size

and concentration of particles or mainly organisms seems to be the important contributor to the changes in backscattered light intensity. The scattering intensity of suspended particles is proportional to λ^{-n} where λ is the wavelength and n the Rayleigh value which may vary from 4 for pure water to 0 at high turbidity. In other words the intensity of backscattered light increases with particle concentration. This shows the important influence of particles without chlorophyll on the backscattered light from below the sea surface.

The Earth Resources Technology Satellite carried a multispectral scanner (MSS) which recorded outgoing radiance in four channels with the following spectral bands:

Channel 4	0.5 to 0.6 µm
Channel 5	0.6 to 0.7 µm
Channel 6	0.7 to 0.8 µm
Channel 7	0.8 to 1.1 µm

With increasing wavelength the photopenetration depth decreases. That means that any response in channel 7 defines a very near surface feature or atmospheric contribution (clouds). This allows us to use channel 7 as a cloud discriminator to judge whether the field of view of the MSS is cloudfree or not.

In respect to ERTS-1 recordings the maximum energy backscattered from plankton or organisms is covered by the two channels between 0.5 and 0.6 µm and 0.6 to 0.7 µm. But extremely high concentrations of plankton should be visible in other channels, too. This has been demonstrated by Szekielda and Curran (1972). The test site which was chosen for the biomass studies with ERTS-1 is between 10°N and 32°N. A composite of ERTS-1 imageries is

given in Fig. 14.

We might conclude that most energy from the backscattered light from below the surface is due to the plankton organisms and probably affected by a certain degree by chlorophyll. This information can be correlated with biomass or plankton concentrations.

One intense and strong upwelling along the NW Coast of Africa appears between Cape Sim and Cape Ghir. One survey made in July 1972 showed the lowest temperature down to 14.5°C. Furnestin (1948) reported data from July and August 1947 with temperatures not below 16°C for the same area. The horizontal chlorophyll and temperature distribution as obtained with the research vessel "Jean Charcot: is shown in Fig. 15. The coldest water is located between 30°N and 31°31'. In accordance with the temperature data the highest chlorophyll concentration was greater than 3.5 $\mu g \cdot l^{-1}$ and was found in the same location. The discrete sampling of the data over a period of four weeks smooths out many of the details which might appear in the real distribution of chlorophyll and other surface parameters. Continuous recordings of chlorophyll, temperature and nutrients showed that the distribution of these parameters is much more structured than indicated by the analysis of discrete samples (Fig. 16). For the July period no satellite coverage was obtained.

Recordings in the visible with ERTS-1 during August and February showed still the exist nce of plankton and/or high chlorophyll concentrations Fig. 17 shows the patchiness in plankton distribution as recorded by ERTS-1 on February 20, 1973. The left hand side shows the recorded energy

in the green band as a pictorial display. The position of the frame is shown in the right hand side of the image composite. In the spectral region between 0.5 to 0.6 μm, the water has the highest photon penetration depth. Therefore an integrated value for plankton over the penetration of light will be received.

The corresponding imagery from the red band of the multispectral scanner is displayed in Fig. 18. Since the photon penetration depth is lower than in the green band, only near surface phenomena will be observed. The interpretation of this frame showed two cyclonic gyres at Cape Hadid, and another gyre near Cape Sim. With different enhancements of the original negative, more detailed analysis of this current system was achieved. The right hand side of Fig. 18 shows the near surface circulation as derived from channel 5. It has to be stressed that this analysis shows only the near surface features and it is questionable whether these surface currents reflect also the circulation in the deeper layers. Repeated coverage of the area indicated that the direction of the surface currents is not permanent. Furnestin (1970) also showed seasonal variation in different planktonic species which is an indication for the change in intensity of upwelling.

Fig. 19 is an image which was recorded on February 20, 1973, near Cape Ghir. It shows the recordings in channel 4 which has its maximum spectral response between 0.5 and 0.6 μm. A similar approach as shown in Fig. 18 was undertaken to analyze different enhanced imagery material for the current pattern. The surface movements of the water masses showed similar

complicated structure in the patterns.

Since the backscattered light from plankton is most effectively in the green part of the electromagnetic spectrum the different gray shades over the oceans can be interpreted in terms of plankton concentration. The ERTS data showed that two different active upwelling cores with high concentration of plankton appear between 30°N and 31°N. Continuous recordings of chlorophyll in the surface water confirmed the presence of two well developed chlorophyll maxima between Cape Ghir (30°39'N; 09°57'W) and Cape Tefeney (31°05'N; 09°51'W). This is shown in Fig. 20. The chlorophyll concentration near Cape Ghir reached 4 $\mu g.l^{-1}$ and at Cape Tefeney 1.6 $\mu g \cdot l^{-1}$. Data reported by Furnestin (1959) also suggest these separated upwelling areas.

Fig. 21 shows the distribution of surface chlorophyll during August 1972 as measured by the Spanish vessel "Cornide de Saavedra" and the English ship "Discovery" simultaneously. High concentrations of chlorophyll according to the discrete samples, were found near Cape Juby. Concentration on the near coastal stations showed chlorophyll up to 8 $\mu g \cdot l^{-1}$. Continuous recordings of fluorescence detected maximum values of 16 $\mu g \cdot l^{-1}$. Outside the upwelling area concentrations were below 0.1 $\mu g \cdot l^{-1}$.

High concentrations of chlorophyll were also found between Cape Barbas and Cape Blanc. During the investigations in August 1972, Cape Juby was covered with one frame by ERTS. Distribution of temperature and chlorophyll in a section perpendicular to the coast near Cape Juby is shown in Fig. 22. The surface temperatures are below 16.5 C and showed the lowest vertical

gradient in the near coastal waters. The distribution is similar to that described by Mascareno and Molina (1970). In the upwelling center, chlorophyll reached concentrations above 0.7 $\mu g \cdot l^{-1}$. Ship measurements and satellite data are compared in Fig. 23, where continuous chlorophyll recordings at the surface were compared with ratios between the channels 4 and 5. Both analysis showed similar patterns although they were three days apart.

The area between Cape Blanc and Cape Timerife shows during the entire year low albedo levels (see Fig. 6). The analysis of data recorded by ERTS-1 in channel 7 showed no clouds in the frame which is shown in Fig. 24. The pictorial display of the green band can therefore be used for an interpretation of the distribution pattern in plankton. Recording in the red band in Fig. 25 still showed backscattered light from organisms. This indicates that higher concentration of plankton is found near to the surface. Chlorophyll concentration for August was found by Margalef (1971) to be 8 $\mu g \cdot l^{-1}$ near Cape Blanc. Productivity data reported by Furnestin (1970) shows that the Cape Blanc region is much more productive than the other upwelling areas:

Region	$gC/m^2/day$
Off Cape Blanc	0.55 - 0.67
Cape Verde	0.11 - 0.24
Canaries	0.034 - .036

Repeated coverage of the test site between Cape Blanc and Cape Timiris showed the changes in the position of the plankton maxima.

A similar approach to obtain the current pattern as made for the Cape Sim area was done with enhancement of the channels 4 and 5. By enhancing

different gray levels, the qualitative information on direction and transportation of the plankton blooms was established. This analysis of channels 4 and 5 for February 22, 1973, is shown in Fig. 26 where the main transportation of plankton was offshore. The near coastal areas showed very low concentration in plankton. The time necessary for the growth in plankton algae might be expected far from the center of upwelling, confirmed by the high reflected energy in the offshore region.

Data from NOAA-2 satellite were analyzed for the same day (Fig. 27). The digitized data for the red band and the infrared which were calibrated in terms of temperature, are given on the left hand side in Fig. 27. The shaded area represents high concentrations of plankton as indicated by the reflected energy. The shaded areas in the infrared recordings show blackbody temperatures below 290° Kelvin. The temperature was not corrected for atmospheric attenuation but patchiness in the temperature distribution can be used to locate the origin for the place where the coldest water was found. A correction to be added for NOAA-2 data due to atmospheric attenuation is about four degrees for a blackbody temperature of 290° Kelvin. This would result in a temperature of 21°C in the center of cold water. The surrounding temperatures are four to six degrees higher compared to the coldest water. This analysis showed that the lowest temperature is away from the coast. But with a single orbit alone it is not possible to decide whether the cold water represents an intrusion from another area or new locally upwelled water.

5. CONCLUSIONS

From the analyzed spacecraft data it is obvious that the distribution of temperature and non-conservative parameters is much more complicated than one might expect from conventional measurements onboard a ship. The variability of oceanographic parameters (see for instance, Jones, 1972; Ballester, et al., 1972) can hardly be resolved on a large scale even if continuous recordings are applied. The advantage of satellite coverage in a test site like the NW Coast of Africa is a fast detection of surface phenomena and the possibility of repeated observation for a relatively low price.

The presented data should help to design future experiments in respect to the heterogeneity and fast changes of the environment as detected from space. Aircrafts and/or spacecrafts data should be made available on a real-time base to assure the most effective experimentation with ships.

ACKNOWLEDGEMENTS

This research was sponsored by NASA under Contract No. NAS5-21784.

I would like to acknowledge the help of many of my colleagues who contributed to the program. Within the CINECA program, space on research vessels was made available to collect ground truth data through Dr. A. Thiriot, France, and Dr. G. Cabrera, Spain. Data exchange was initiated with Dr. K. F. Bowden, England, and Dr. W. Nehring, German Democratic Republic. Figs. 11 and 12 are part of a program to measure and compare satellite data with ship observations. Dr. J. Leese from NESS is contributing the digitized data from NOAA-2. Dr. A. Strong provided the digitized data in Fig. 27. Data used for the graph in Fig. 14 were recorded by Dr. W. Hovis, GSFC.

Dr. R. Curran, NASA Goddard Space Flight Center contributed significantly with his research and discussions. Technical help has to be acknowledged to Mrs. E. Ganzman, J. Schaefer, M. Maerker, and D. Jay, at CMS, and Mrs. L. Regalla for computer work during my stay at NASA as a National Academy of Sciences - Associate.

FIGURE CAPTIONS

Fig. 1: Infrared recorded imagery along the NW Coast of Africa between 30°N and 5°N. The continent and the Cape Islands appear black. Clouds are displayed in white. Data obtained with Nimbus IV Temperature Humidity Infrared Radiometer (THIR) on 24 June 1970 in the atmospheric window at 11.5 µm.

Fig. 2: Data obtained with the Image Dissector Camera System (IDCS) on Nimbus III between 10°N and 35°N on June 15, 1969.

Fig. 3: The Northwest Coast of Africa between Cape Juby and Rio de Oro as viewed during a Gemini flight.

Fig. 4: Solar reflected energy as recorded along the NW Coast of Africa and Spain by ITDS on 15 April 1970. The image was recorded in the direct read out mode by the director of "Sternwaite der Stadt Bochurn" H. Kaminski.

Fig. 5: The wind field between Presqu'ile and Cape Verde. Reconstructed from Rossignol and Aboussouan (1965).

Fig. 6: Albedo measurements along the NW Coast of Africa over a two week period in June 1970.

Fig. 7: IDCS-picture (left) and infrared image (right) taken on 18 April 1970. For explanation see text.

Fig. 8: IDCS-picture (left) and infrared image (right) taken on 20 April 1970. For explanation see text.

Fig. 9: IDCS-picture (left) and infrared image (right) taken on 22 April 1970. For explanation see text.

Fig. 10: IDCS-picture (left) and infrared image (right) taken on 25 April 1970.

Fig. 11: Digital printout of sea surface temperature as obtained with NOAA-2 between 10°N to 30°N, 15°W to 30°W, on 26 April 1973.

Fig. 12: Digital printout of sea surface temperature as obtained with NOAA-2 between 10°N to 30°N, 15°W to 30°W, on 3 May 1973.

Fig. 13: Backscattered energy from the ocean due to particulate and dissolved material.

Fig. 14: Image composite from data obtained with the MSS on ERTS-1 in channel 7 showing the NW Coast of Africa.

Fig. 15: Chlorophyll and temperature distribution during June 1972.

Fig. 16: Continuous chlorophyll, temperature and nitrate recordings. For location of stations see Fig. 6.

Fig. 17: Recorded imagery in the green band of backscattered light from the upwelling area near Cape Sim.

Fig. 18: Radiance recorded in the red band of the MSS on ERTS-1 (left). Current pattern derived from channel 5 (right).

Fig. 19: Cape Ghir viewed by ERTS-1 (left). Right side shows the derived current patterns.

Fig. 20: Continuous chlorophyll recordings between Cape Ghir (left) and Cape Tefeny (right), July 1972.

Fig. 21: Chlorophyll distribution in August 1972. Values in $\mu g \cdot l^{-1}$.

Fig. 22: Vertical distribution of temperature ( ) and chlorophyll ( ) ($\mu g \cdot l^{-1}$) perpendicular to Cape Juby, August 1972.

Fig. 23: Continuous chlorophyll recordings and color ratios obtained with ERTS-1. The position of the stations and recordings which were used for this comparison are shown in the ERTS-1 imagery. (Analysis done by Dr. R. J. Curran, GSFC, NASA).

Fig. 24: Albedo recordings in channel 4.

Fig. 25: Albedo recordings in channel 5.

Fig. 26: Current patterns derived from ERTS-1 observations.

Fig. 27: Comparison between temperature patterns and reflected energy in the red.

REFERENCES

Ballester, A., A. Cruzado, A. Julia, M. Mariquez and J. Salat (1972). Analysis automatico y continyo de las caracteristicas fisicas, qui micas y biologicas del mar. Publs. Techicas Patr. "J. Cierva" 1, 1-72.

Clarke, G. L., G. C. Ewing and C. L. Lorenzen (1970). Spectra of back-scattered light from the sea obtained from aircraft as a measure of chlorophyll concentration. Science 20, 1119-1121.

Curran, R. J. (1972). Ocean color determination through a scattering atmosphere. Applied Optics 11, 1857-1866.

Düing, W. and K.-H. Szekielda (1971). Monsoonal response in the western Indian Ocean. J. Geophys. Res. 76, 4181-4187.

Fedoseev, A. (1970). Geostrophic Circulation of Surface Waters on the Shelf of North-West Africa. Rapp. Proc. Verb. Cons. Int. Expl. Mer. 159: 32-37.

Furnestin, J. (1948). L'Hydrologie cotière du Maroc. Com. Oceanogr. Et. Côtes, Maroc. Bulletin Scientifique 4, 7-28.

_____ (1959). Hydrologie du Maroc Atlantique. Rev. Trav. Inst. Peches. marit. 23, 7-77.

Furnestin, M.-L. (1970). Rapport sur le plancton. Rapp. Proc. Verb. 159, 90-115.

Jones, P. G. W. (1972). The variability of oceanographic observations off the coast of north-west Africa. Deep-Sea Research 19, 405-431.

LaViolette, P. E. and P. L. Chabot (1969). A method of eliminating cloud interference in satellite studies of sea surface temperatures. Deep-Sea Research, 16: 539-47.

Margaleff, R. (1971). Una campaña oceanografica de "Cornide de Saavedra" en la region de aflora-miento del noroeste Africano. Inv. Pesq. 35 (supl.), pags. 1-39.

Mascareno, D. and R. Molina (1970). Contribution a l'étude de l'upwelling dans la zone Canarienne Africaine. Rapp. Proc. Verb. 159, 61-73.

Mittelstaedt, E. (1972). Der hydrographische Aufbau und die zeitliche Variabilität der Schichtung und Strömung im nordwestafrikanischen Auftriebsgebiet im Frühjahr 1968 "Meteor" Forsch.-Ergebnisse Reihe A, 11, 1-57.

Rossignol, M. and M. T. Aboussouan (1965). Hydrobiologie marine côtière de la Presqu'ile du Cap-Vert. Centre Oceanographique de Dakar, 156 pp.

Shenk, W. E. and V. V. Salomonson (1972). A multispectral technique to determine sea surface temperature using Nimbus 2 data. J. Phys. Res. 2, 157-167.

Smith, W. L., K. P. Rao, R. Koeffler and W. R. Curtis (1970). Determination of sea surface temperature from satellite high resolution infrared window radiation measurements. Monthly Wea. Rept. 98: 607-11.

Szekielda, K.-H. (1972a). Upwelling studies with satellites. J. Cons. Mer. 343: 379-388.

_____(1972b). Validity of ocean surface temperatures monitored from satellites. J. Cons. Int. Explor. Mer. 35. (In press).

_____ and R. J. Curran (1972). Chlorophyll structure in the ocean, 139-141. In: Earth Resources Technology Satellite-1, Symposium Proceedings, Goddard Space Flight Center, Greenbelt, Maryland.

_____ and W. F. Mitchell (1972). Oceanographic application of color-enhanced satellite imageries. Remote Sens. Environ. 2, 71-76.

Tomczak, M. (1970). Schwankungen von Schichtung und Strömung im westafrikanischen Auftriebsgebiet während der "Deutschen Nordatlantischen Expedition" 1937. "Meteor" Forsch.-Ergebnisse Reihe A, 7, 1-51.

Warnecke, G., L. J. Allison, L. M. McMillin, and K.-H. Szekielda (1971). Remote sensing of ocean currents and sea surface temperature changes derived from the Nimbus II satellite. J. Phys. Ocean., 1: 45-60.

Weichart, G. (1970). Kontinuierliche Registrierung der Temperatur und der Phosphat-Konzentration im Oberflächenwasser des nordwestafrikanischen Auftriebswasser-Gebiets. Dt. Hydr. Z. 23, 2: 49-60.

Werner, E. and G. A. Branchflower, (1970). The Image Dissector Camera System (IDCS) Experiment, 11-24. In: The Nimbus IV User's Guide. Goddard Space Flight Center, Greenbelt, Md.

Yentsch, C. S. (1960). The influence of phytoplankton pigments on the color of sea water. Deep-Sea Res. 7, 1-9.

ABBREVIATIONS USED

EMR	Electromagnetic Radiation
ERTS	Earth Resources Technology Satellite
THIR	Temperature Humidity Infrared Radiometer
NOAA	National Oceanic and Atmopsheric Administration
IDCS	Image Dissector Camera System
MRIR	Medium Resolution Infrared Radiometer
NASA	National Aeronautics and Space Administration
NESS	National Environmental Satellite Survey
GSFC	Goddard Space Flight Center
MSS	Multispectral Scanner

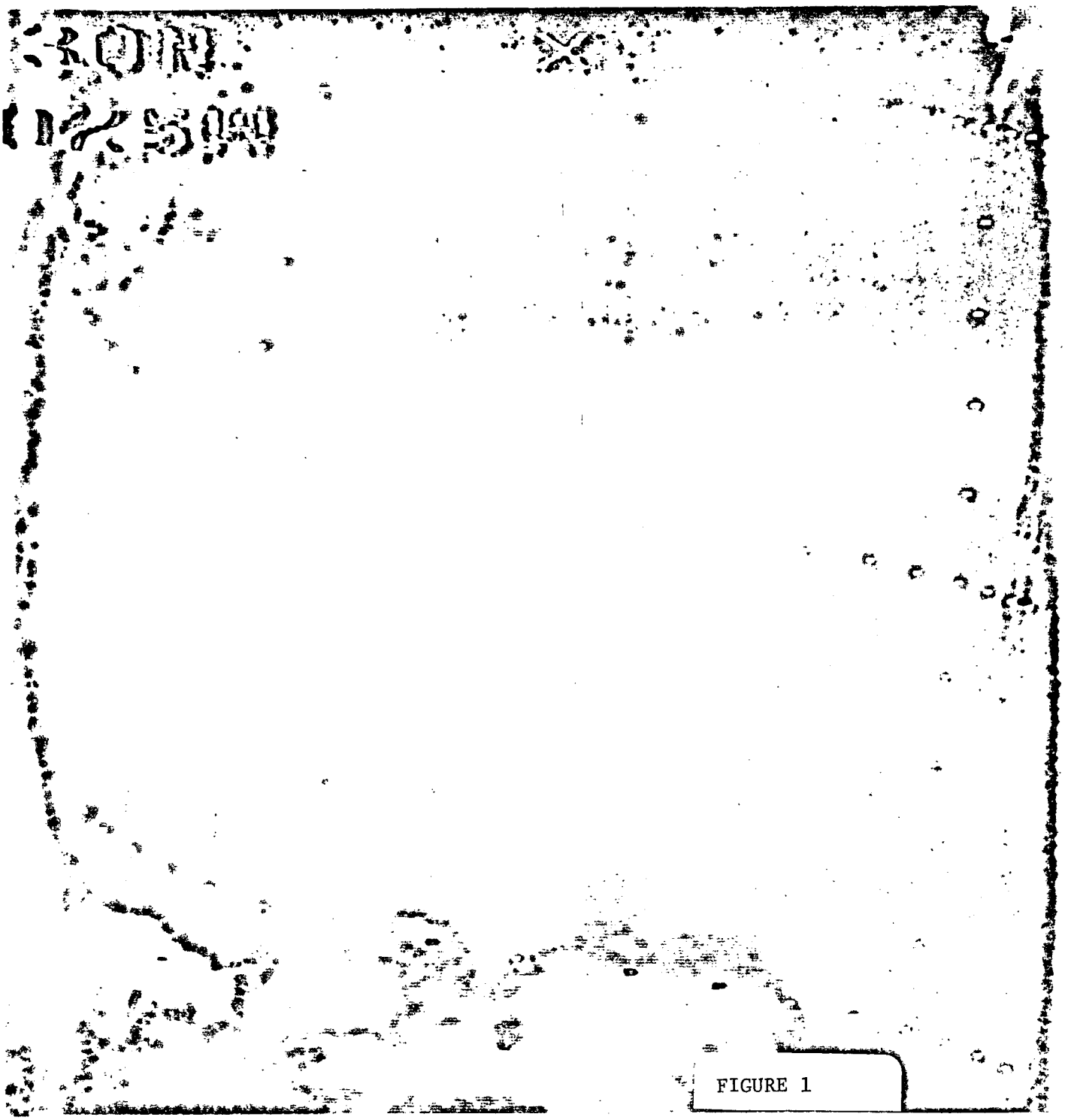

FIGURE 1

FIGURE 2

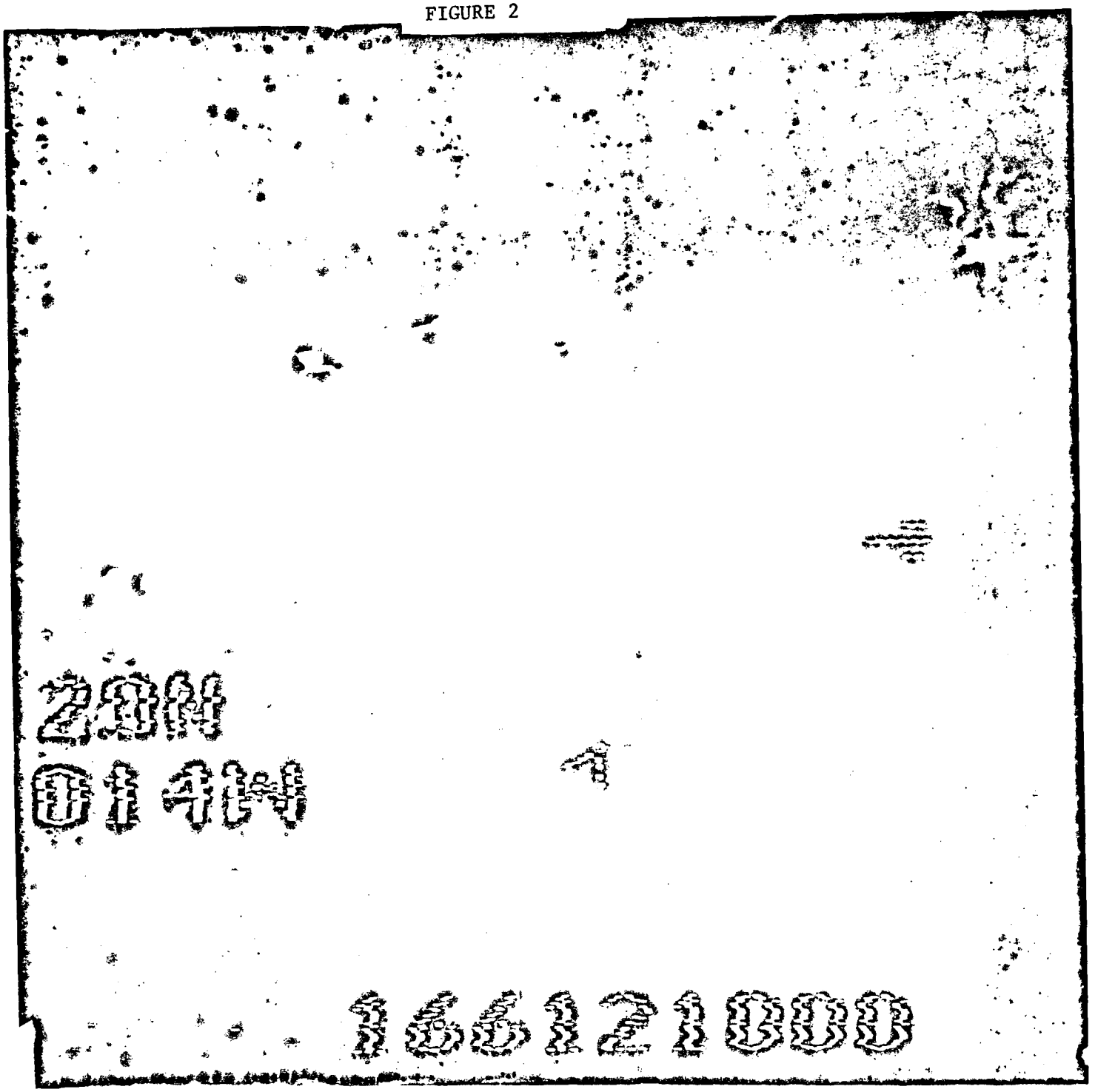

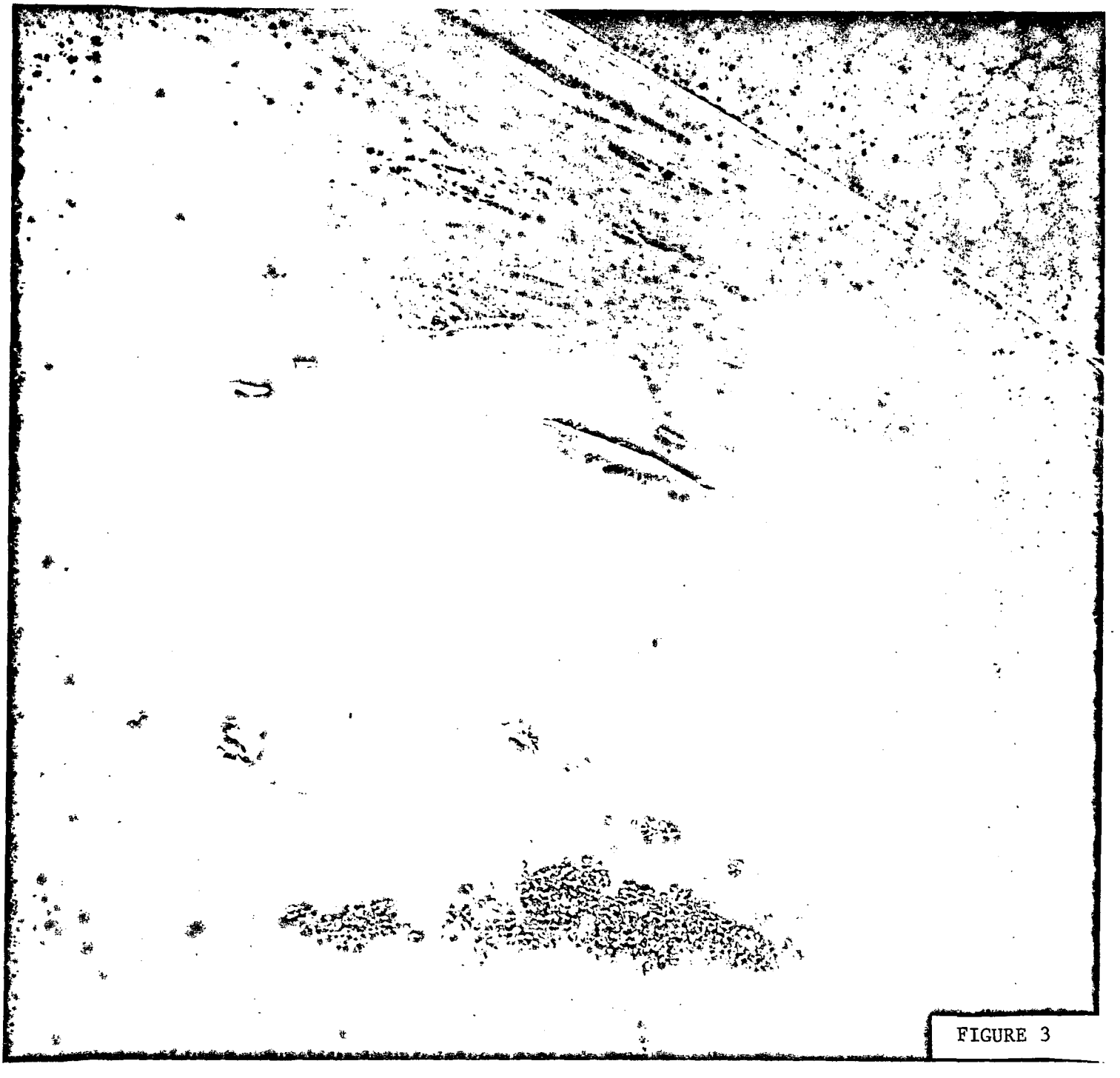

FIGURE 3

FIGURE 4

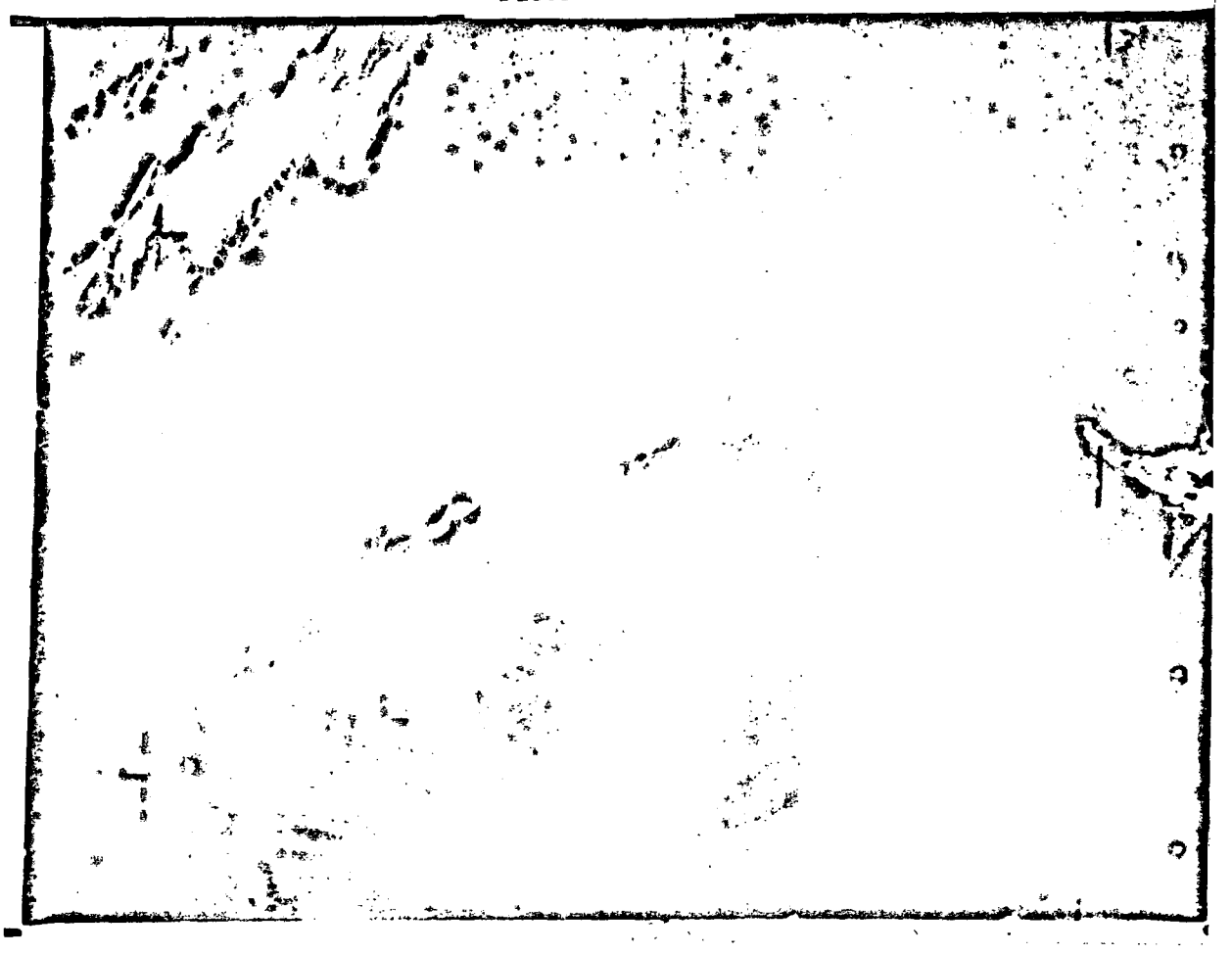

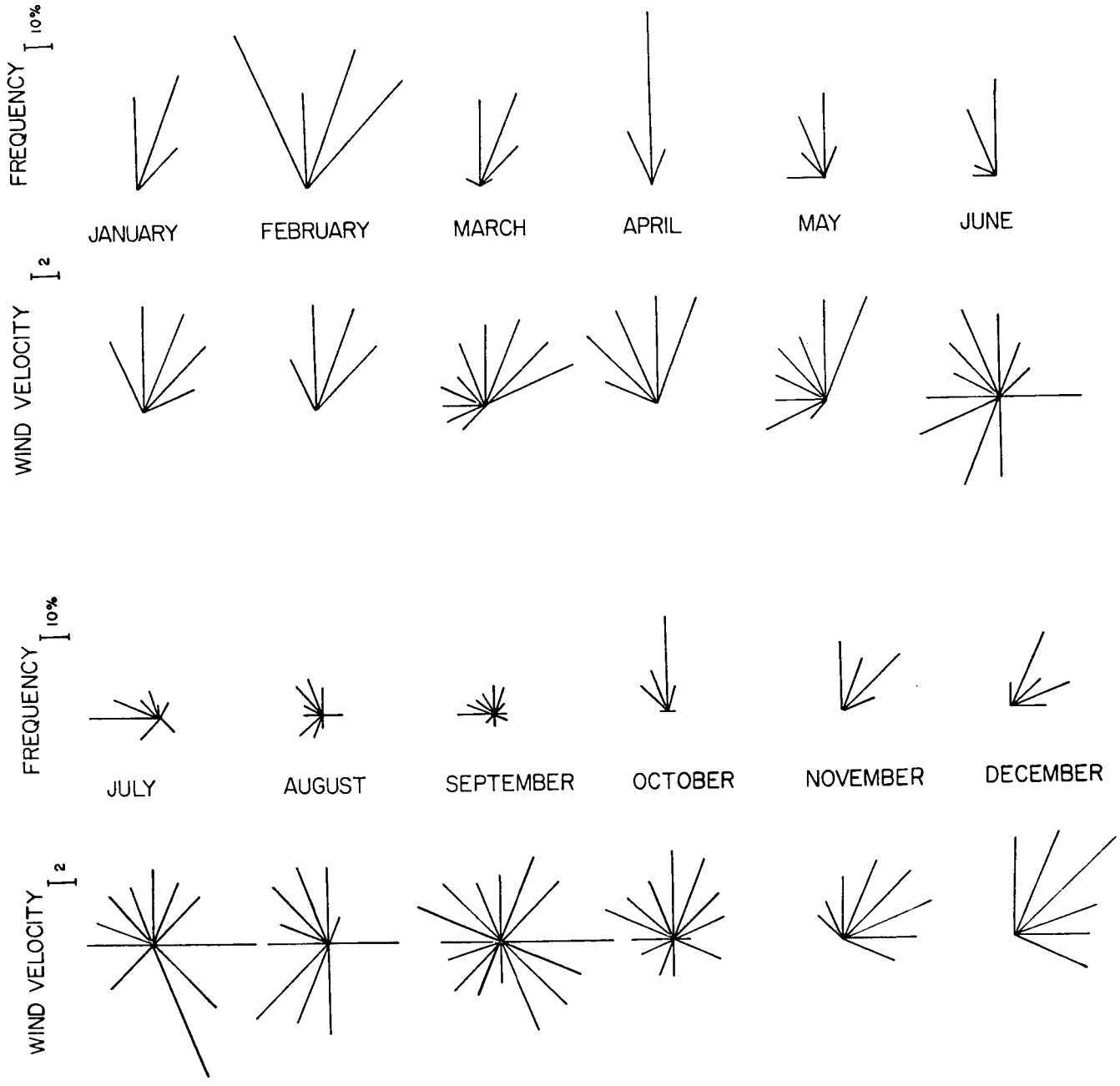
FREQUENCY
10%
JANUARY
FEBRUARY
MARCH
APRIL
MAY
JUNE
WIND VELOCITY
2
JULY
AUGUST
SEPTEMBER
OCTOBER
NOVEMBER
DECEMBER

FIGURE 5

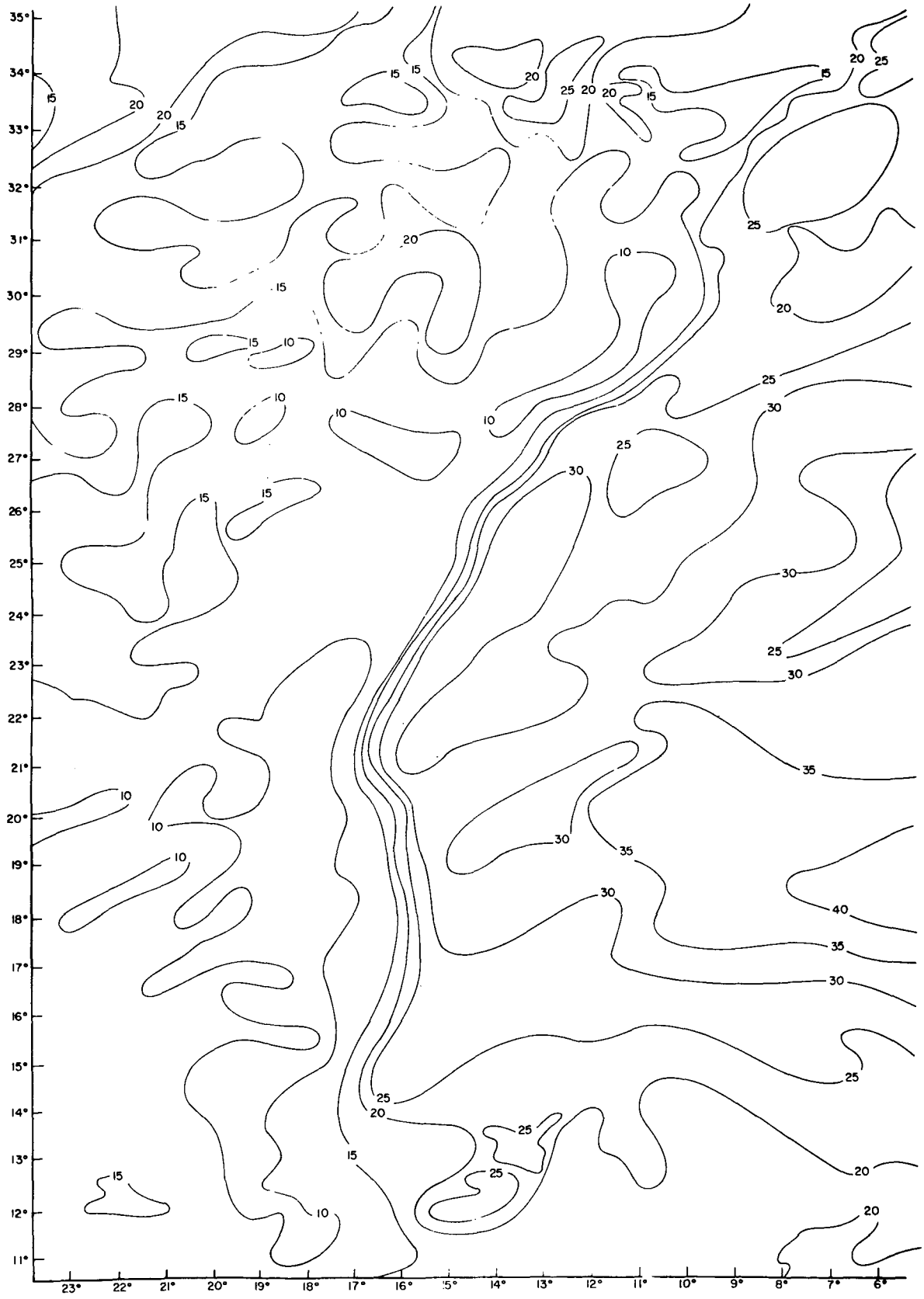
35°
34°
33°
32°
31°
30°
29°
28°
27°
26°
25°
24°
23°
22°
21°
20°
19°
18°
17°
16°
15°
14°
13°
12°
11°
23°
22°
21°
20°
19°
18°
17°
16°
15°
14°
13°
12°
11°
10°
9°
8°
7°
6°

FIGURE 6

18 APRIL 1970

FIGURE 7

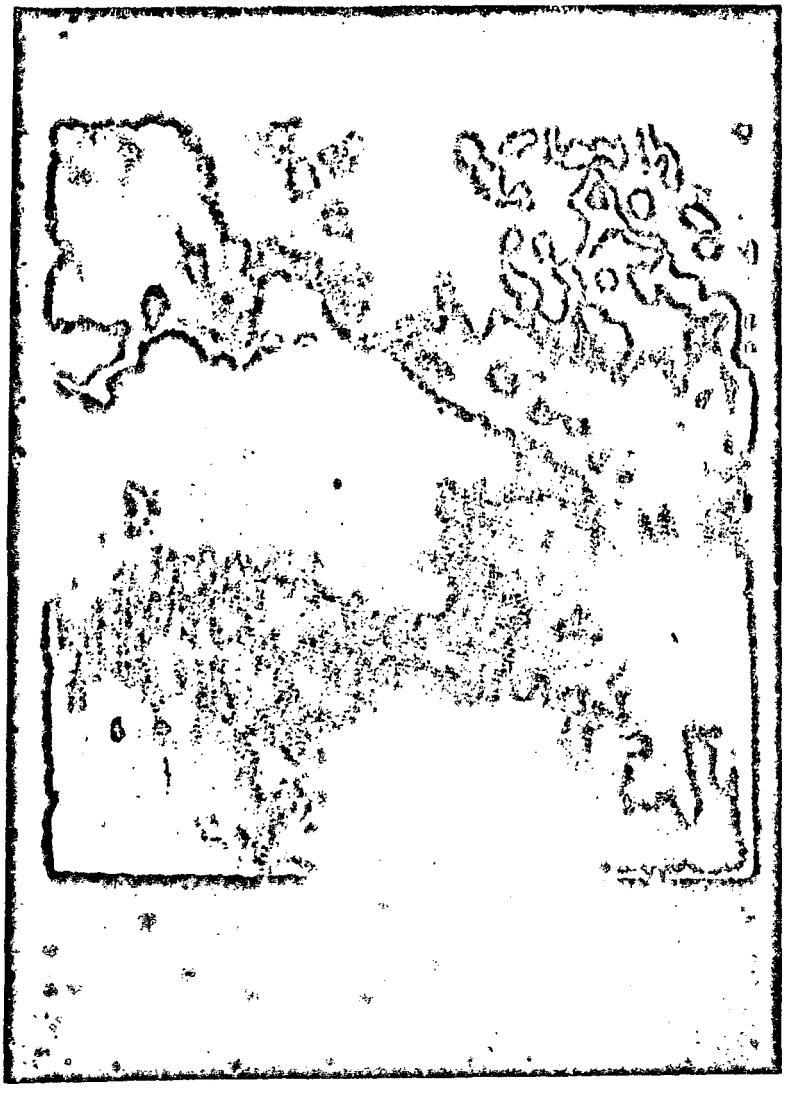

20 APRIL 1970

FIGURE 8

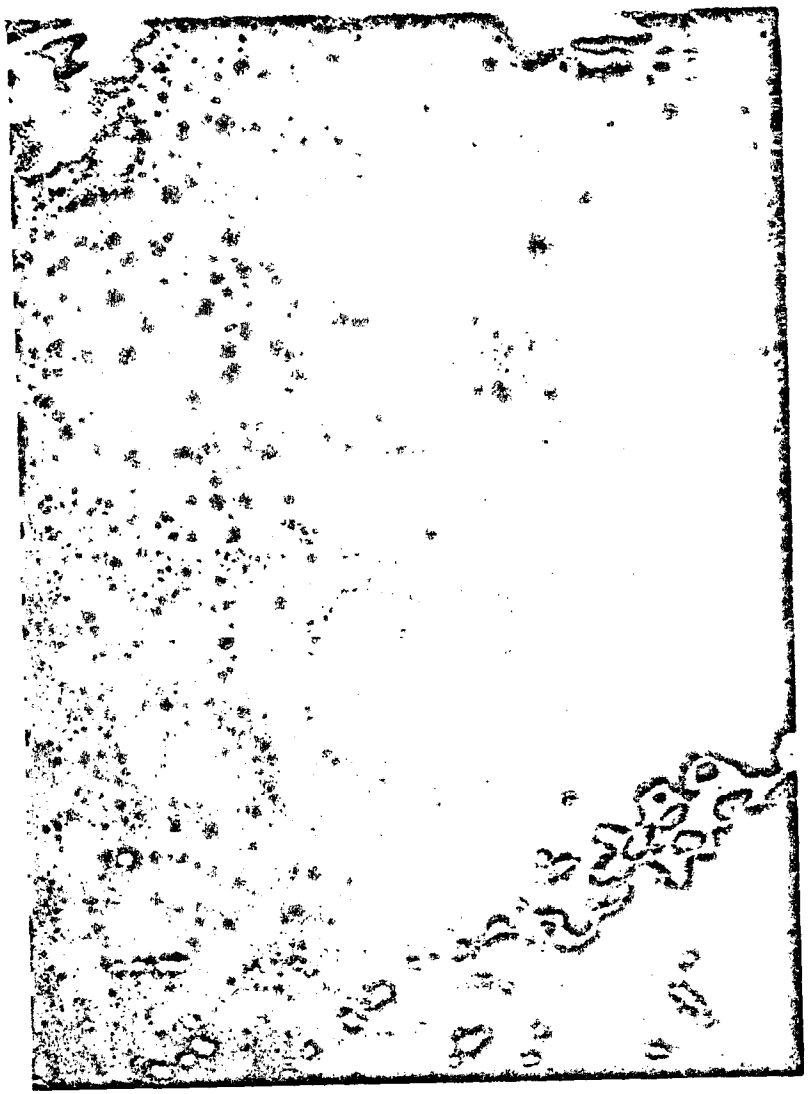

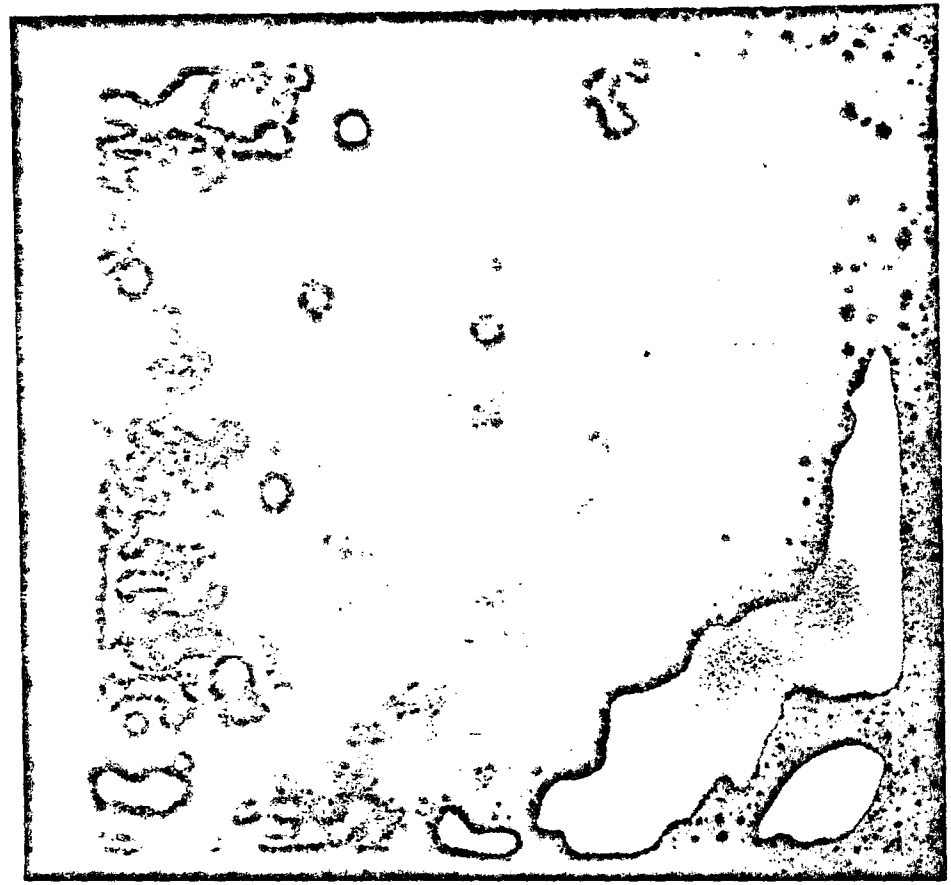

22 APRIL 1970

FIGURE 9

25 APRIL 1970

FIGURE 10

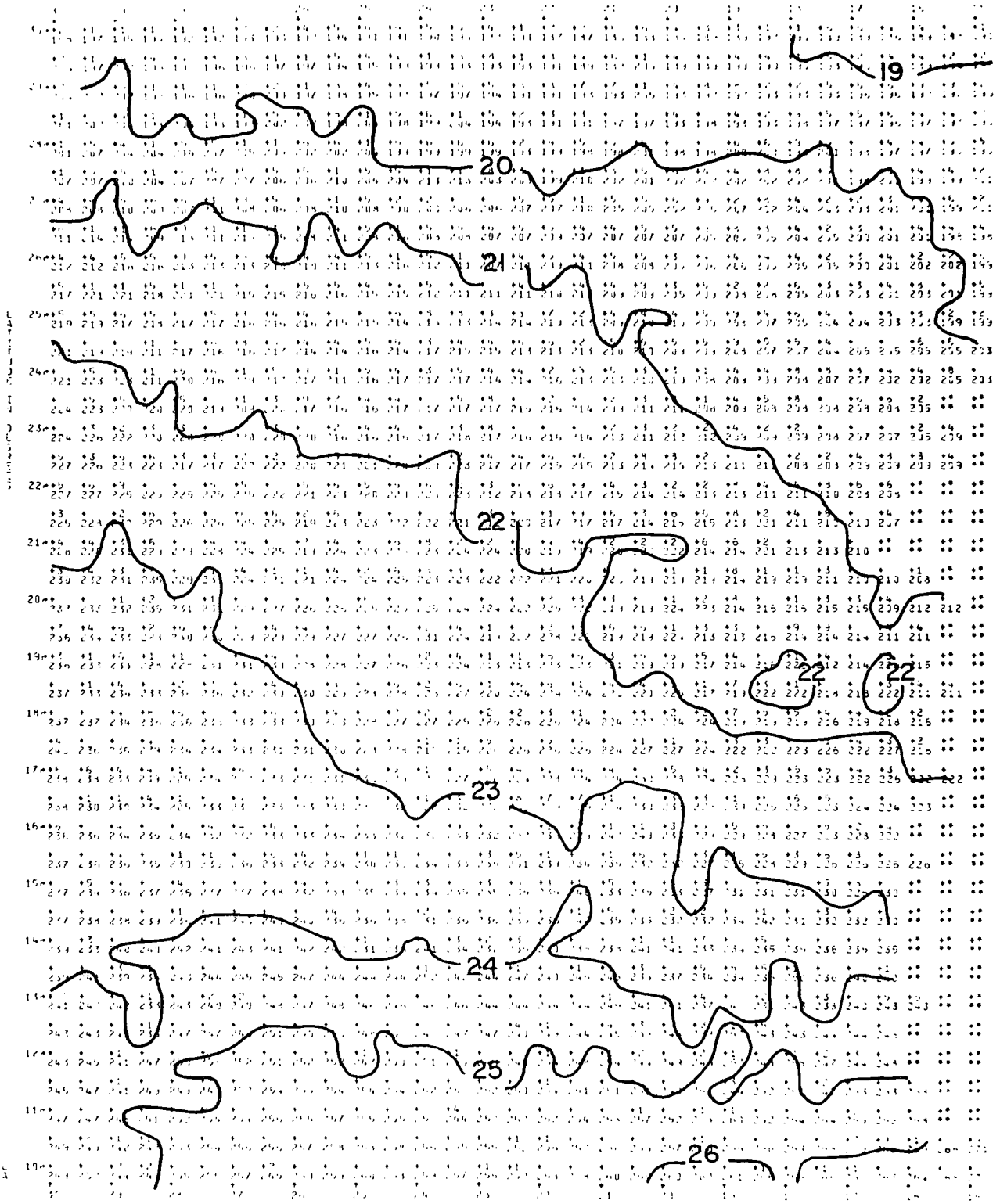

FIGURE 11

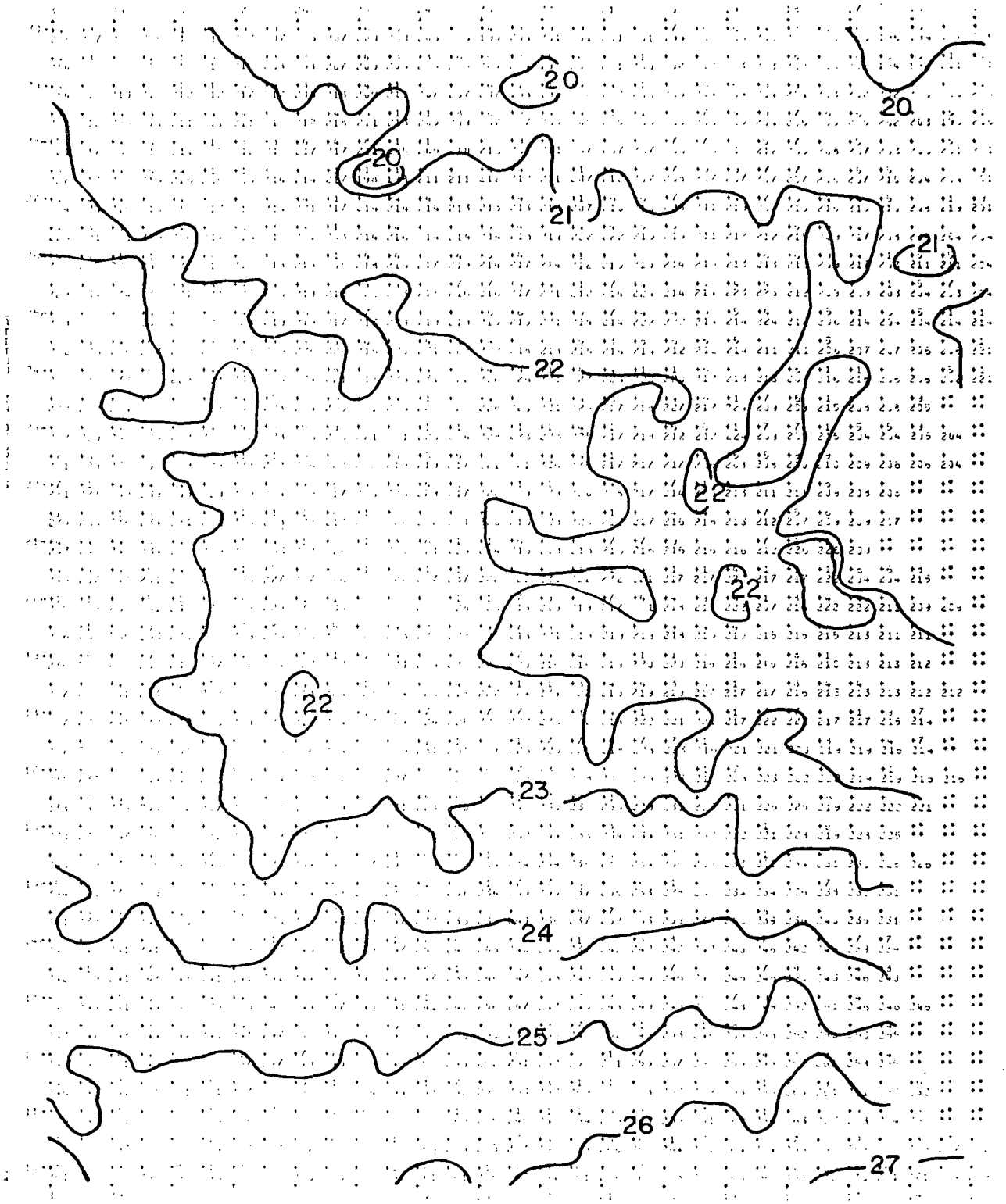

FIGURE 12

FIGURE 13

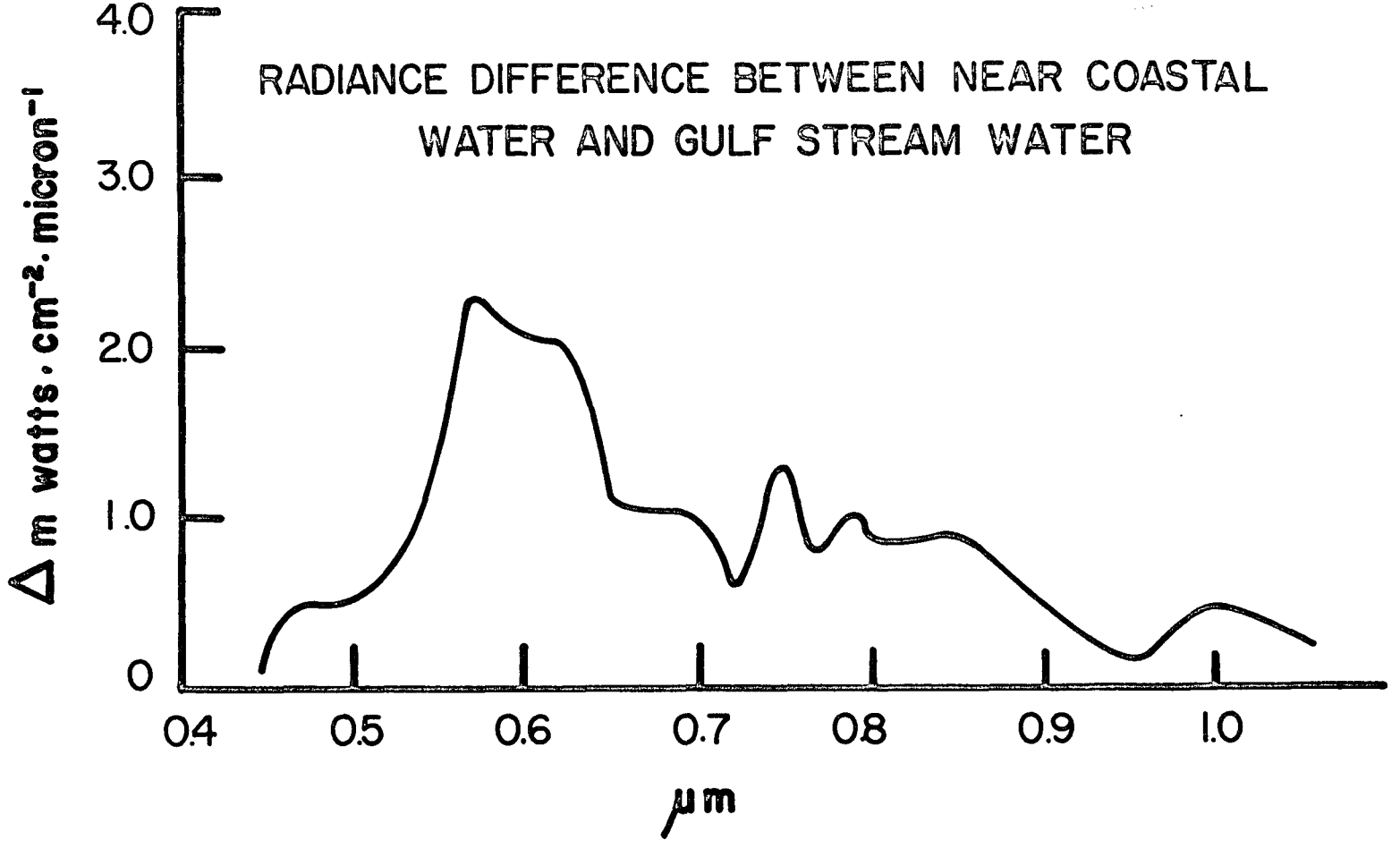
RADIANCE DIFFERENCE BETWEEN NEAR COASTAL WATER AND GULF STREAM WATER
Δ m watts · cm⁻². micron⁻¹
4.0
3.0
2.0
1.0
0
0.4
0.5
0.6
0.7
0.8
0.9
1.0
μm

FIGURE 14

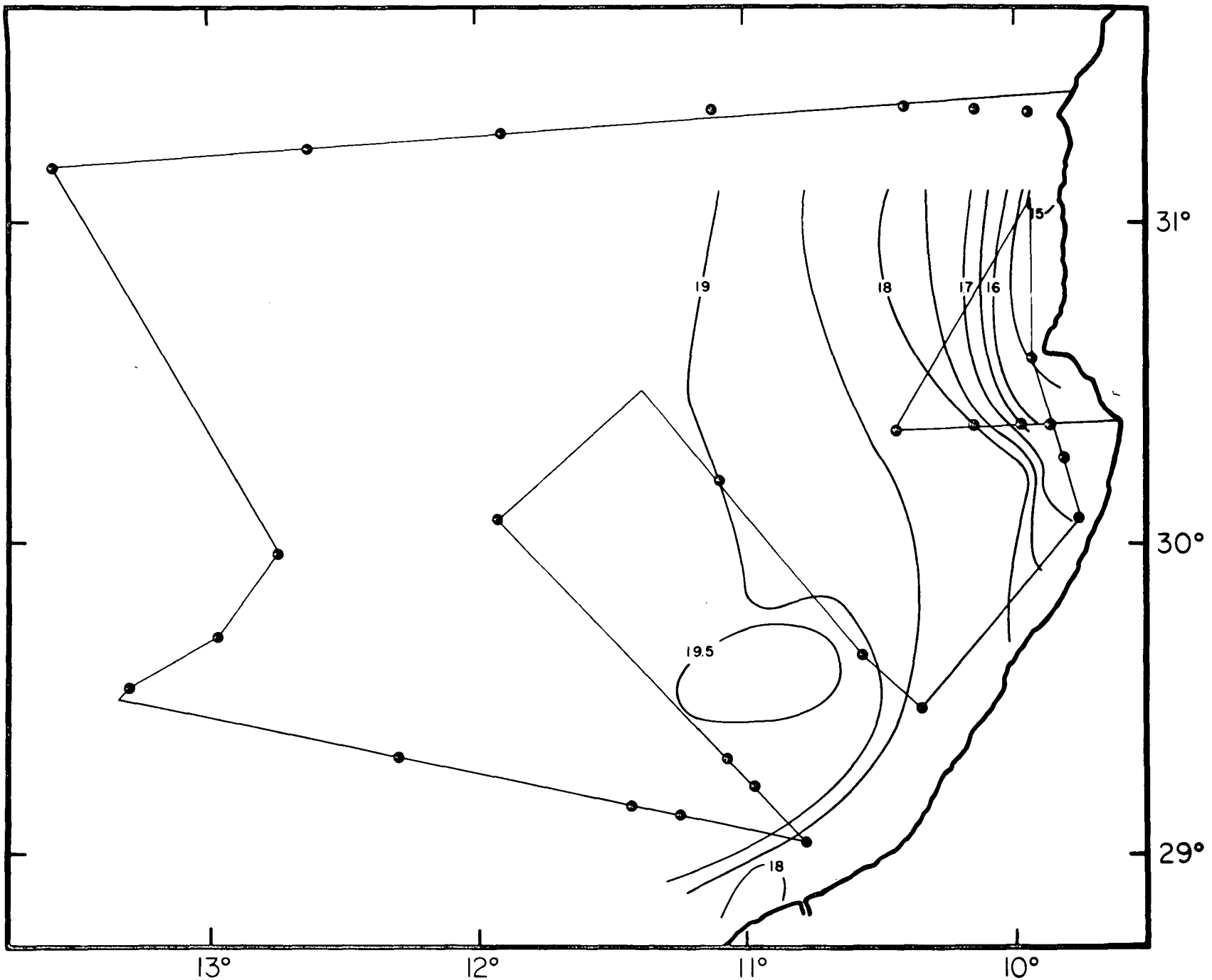

FIGURE 15

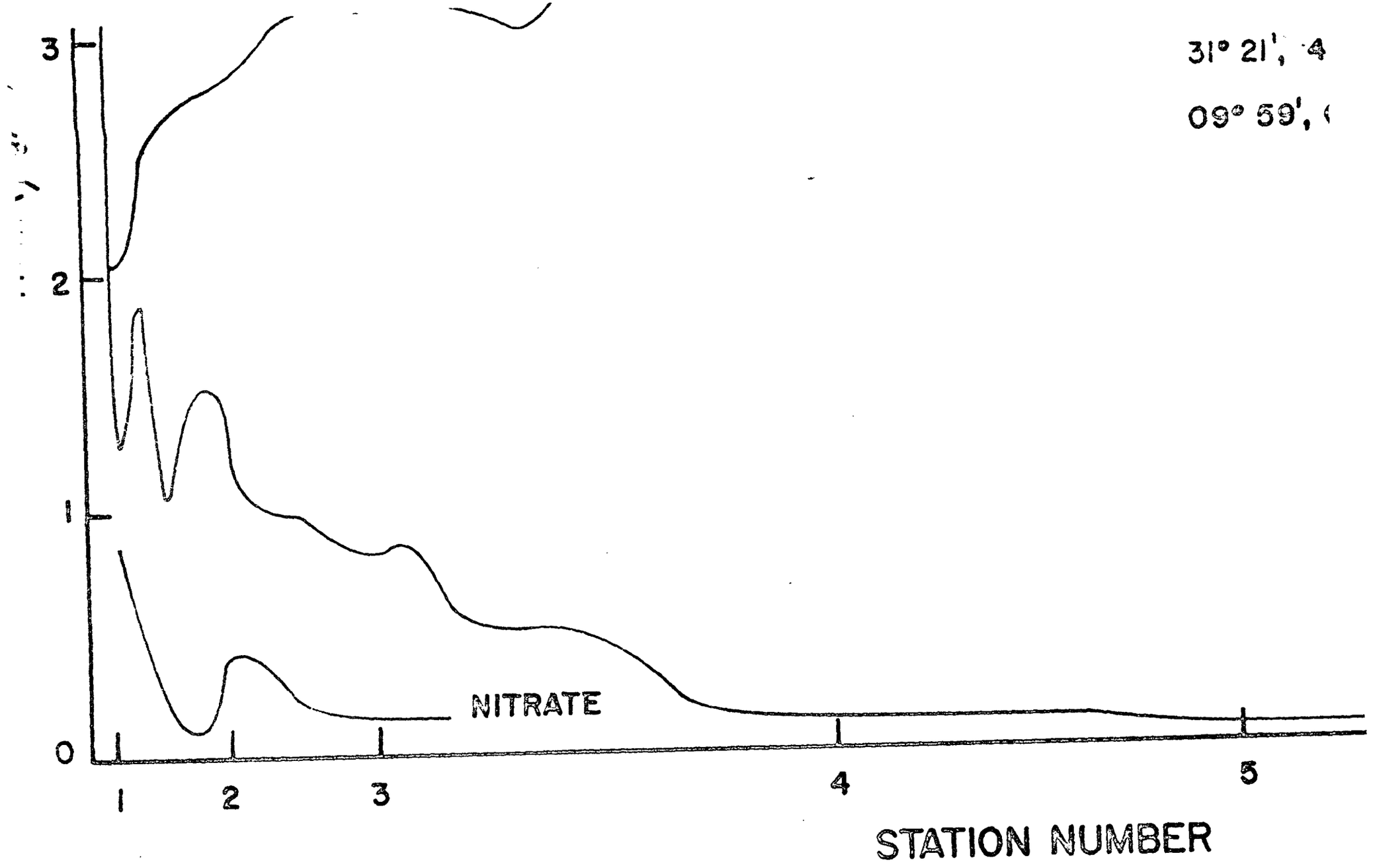

FIGURE 16

UPWELLING & PLANKTON PATTERNS
NORTH-WEST AFRICA

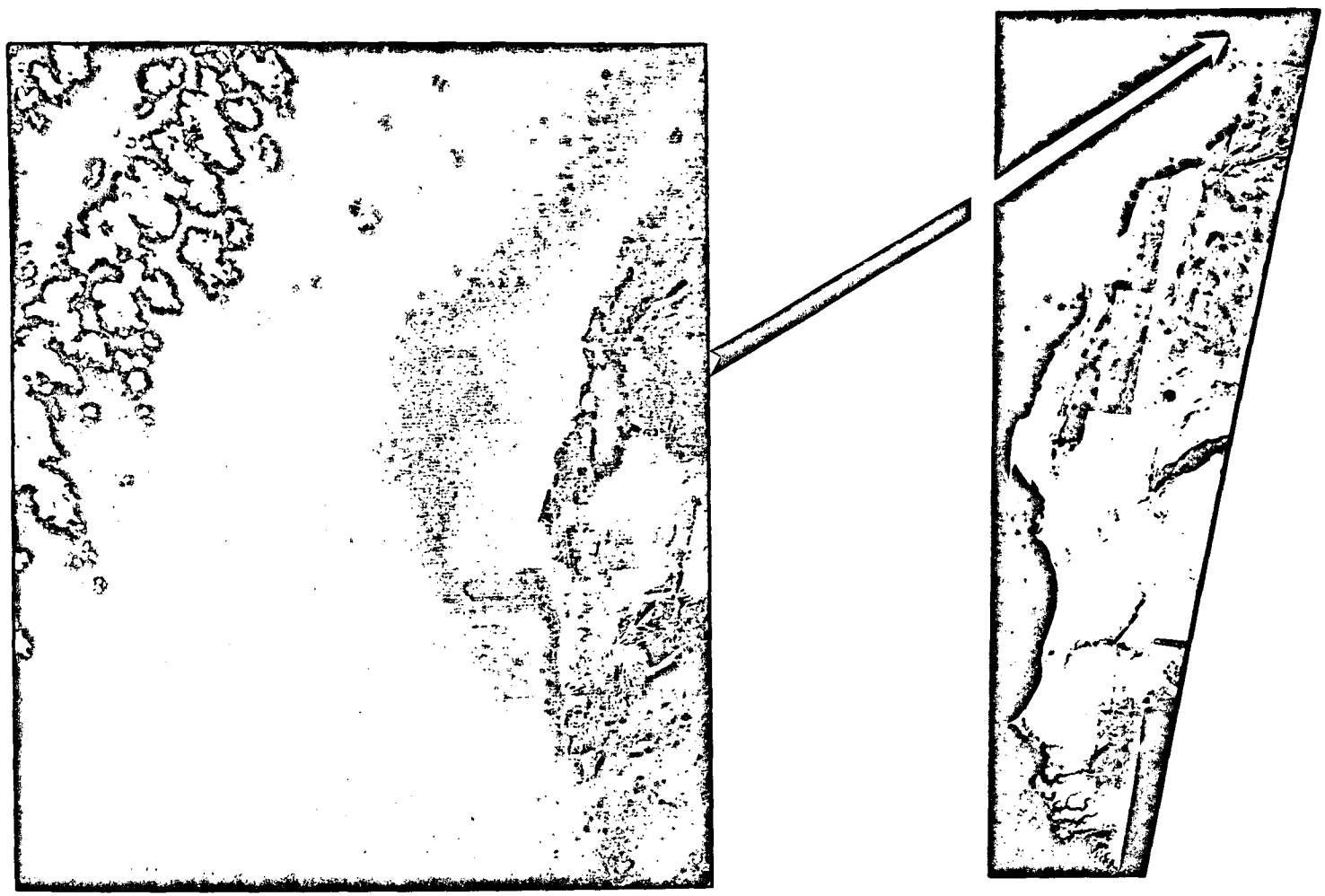

ERTS-1 (GREEN BAND) 20 FEBRUARY 1973

FIGURE 17

GODDARD SPACE FLIGHT CENTER
GREENBELT, MARYLAND

73-9698

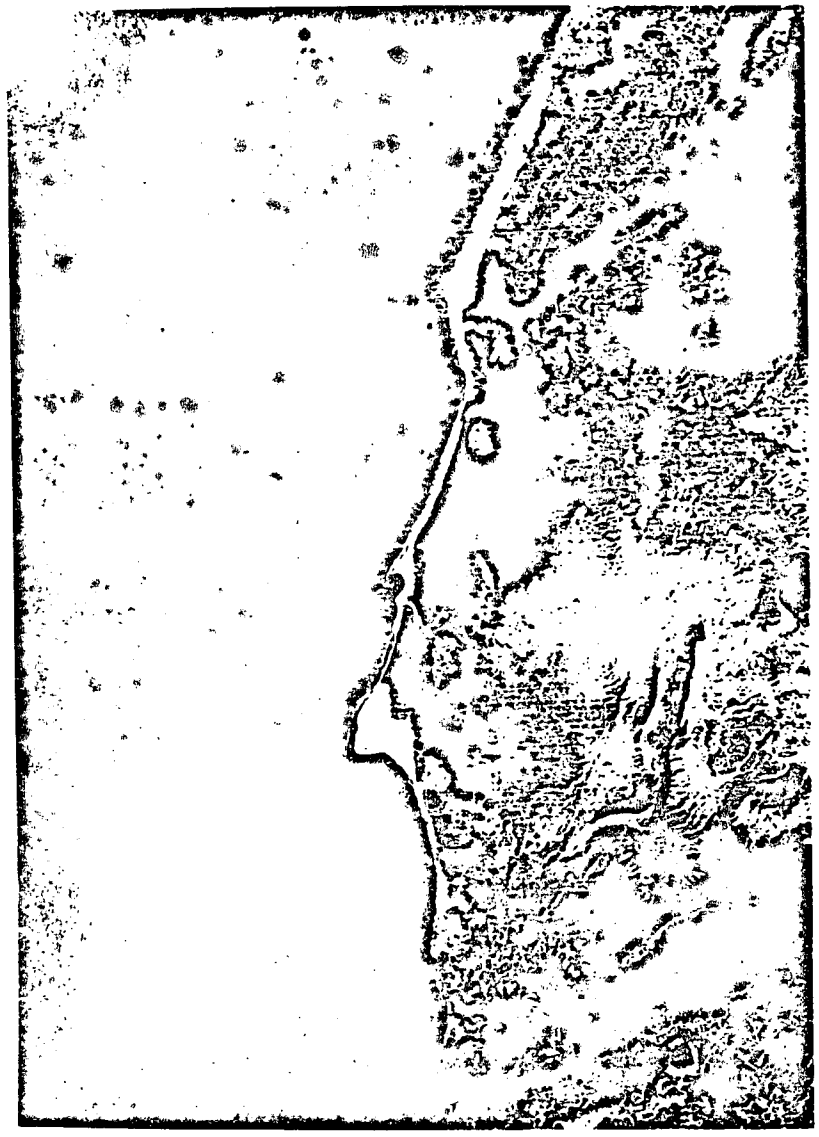

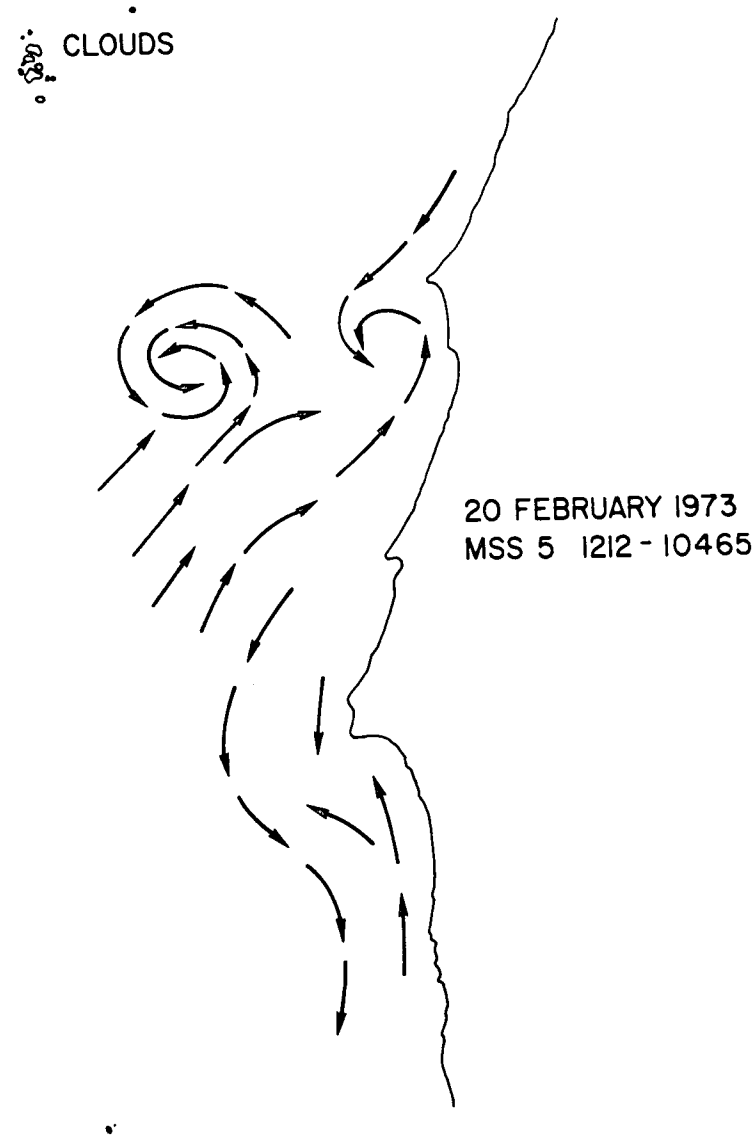

FIGURE 18

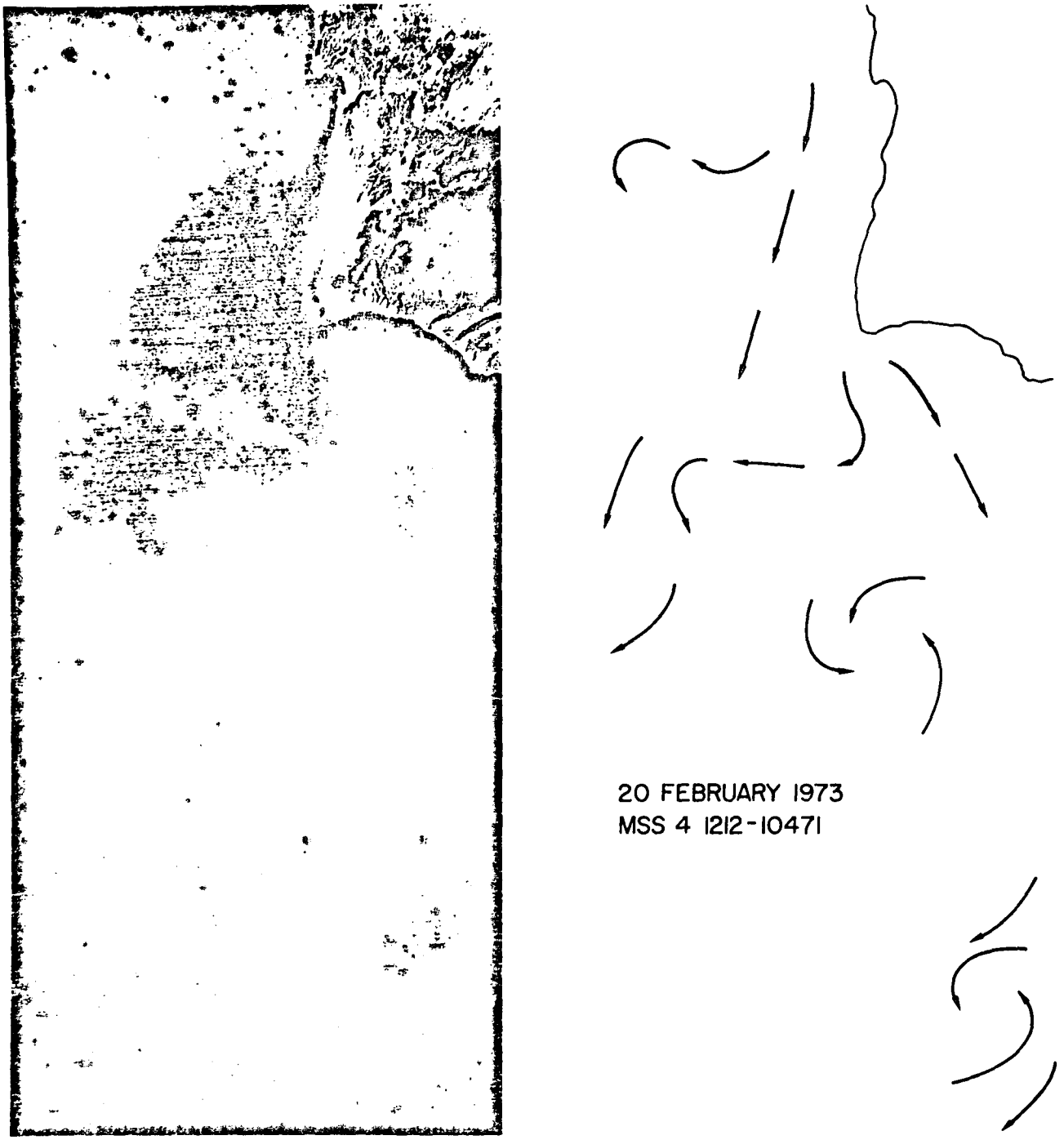

FIGURE 19

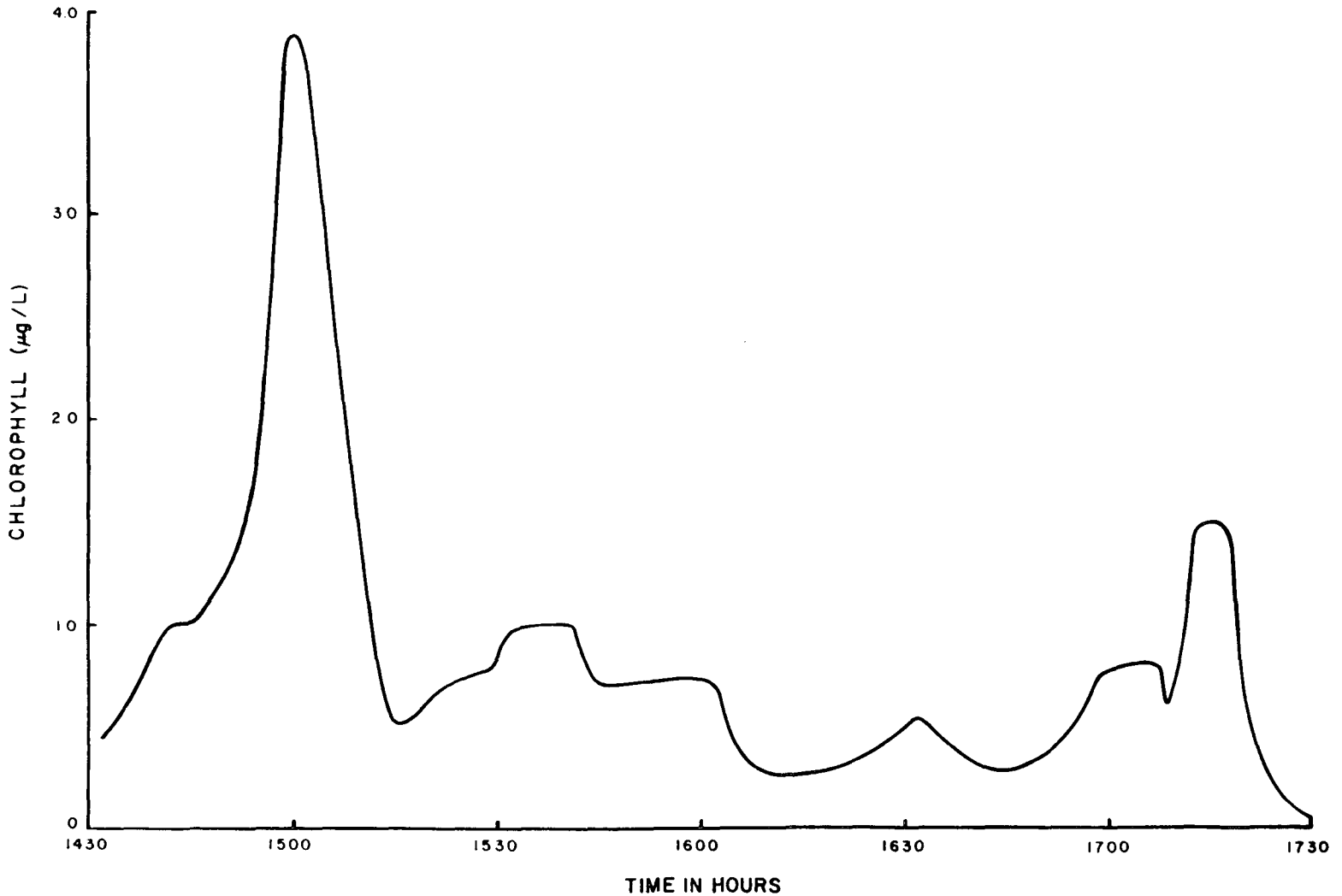
4.0
30
20
10
0
CHLOROPHYLL (µg/L)
1430
1500
1530
1600
1630
1700
1730
TIME IN HOURS

FIGURE 20

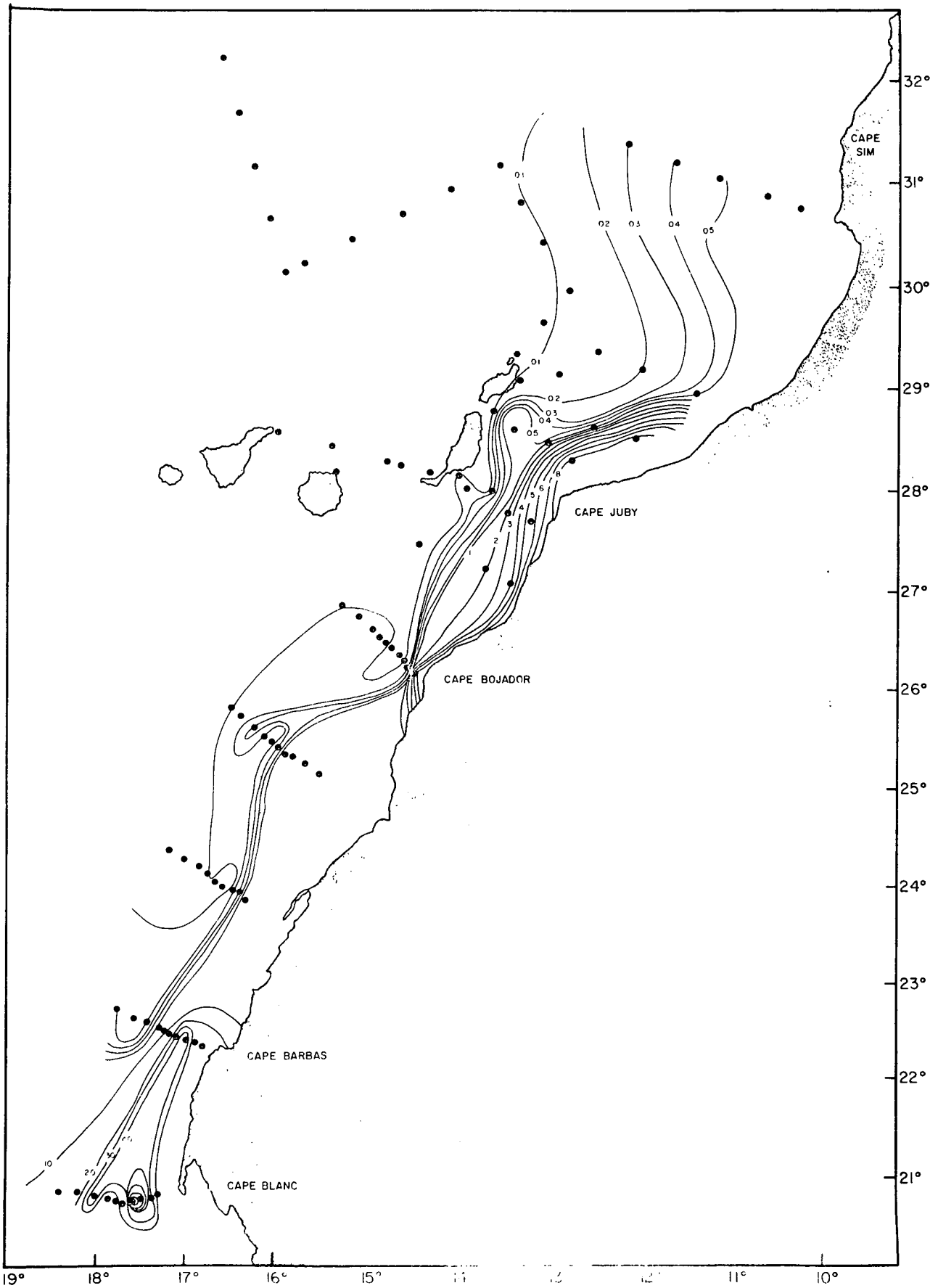
CAPE SIM
CAPE JUBY
CAPE BOJADOR
CAPE BARBAS
CAPE BLANC
01
02
03
04
05
1
2
3
4
5
6
8
10
25
32°
31°
30°
29°
28°
27°
26°
25°
24°
23°
22°
21°
19°
18°
17°
16°
15°
11°
10°

FIGURE 21

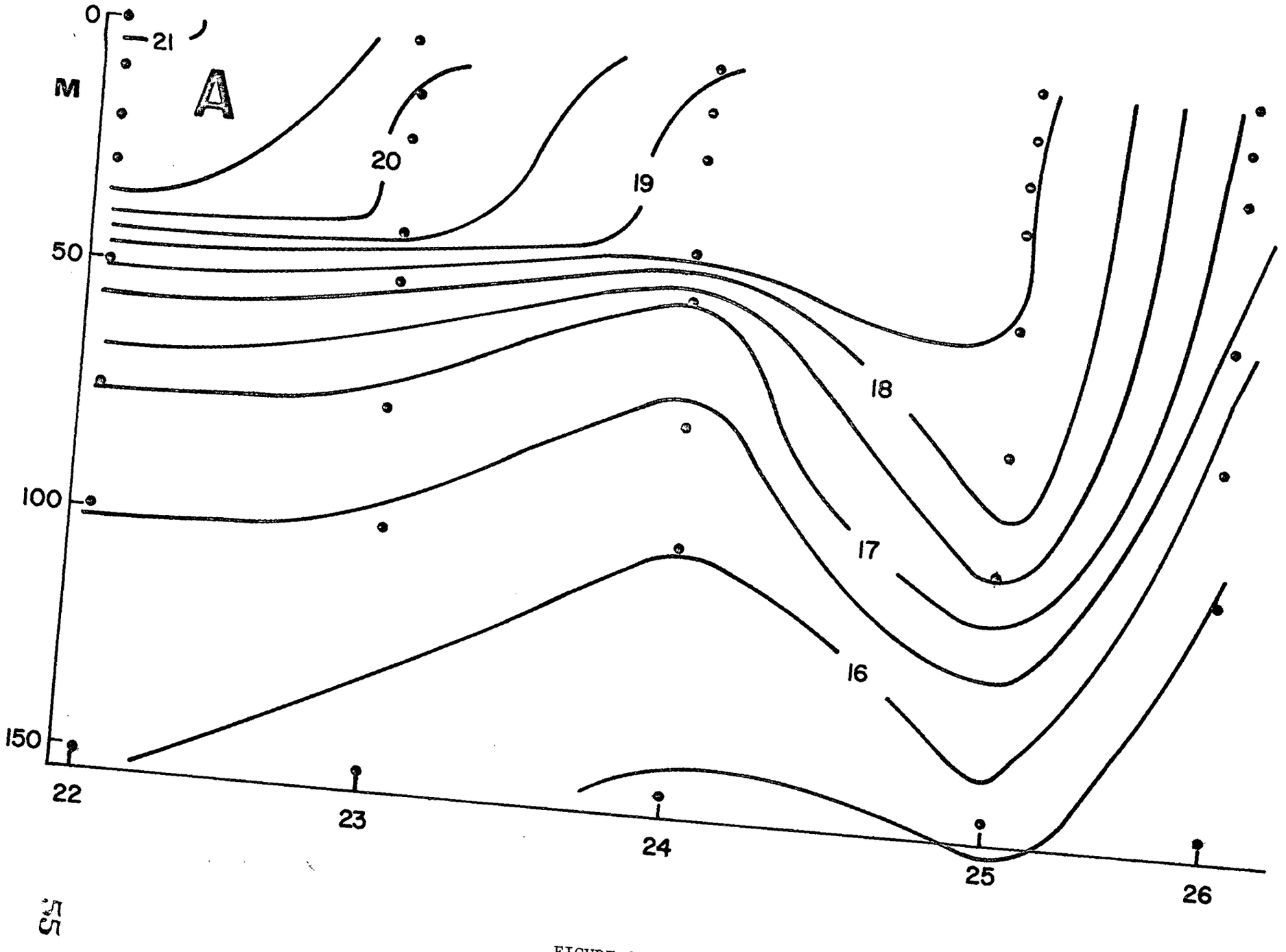

FIGURE 22

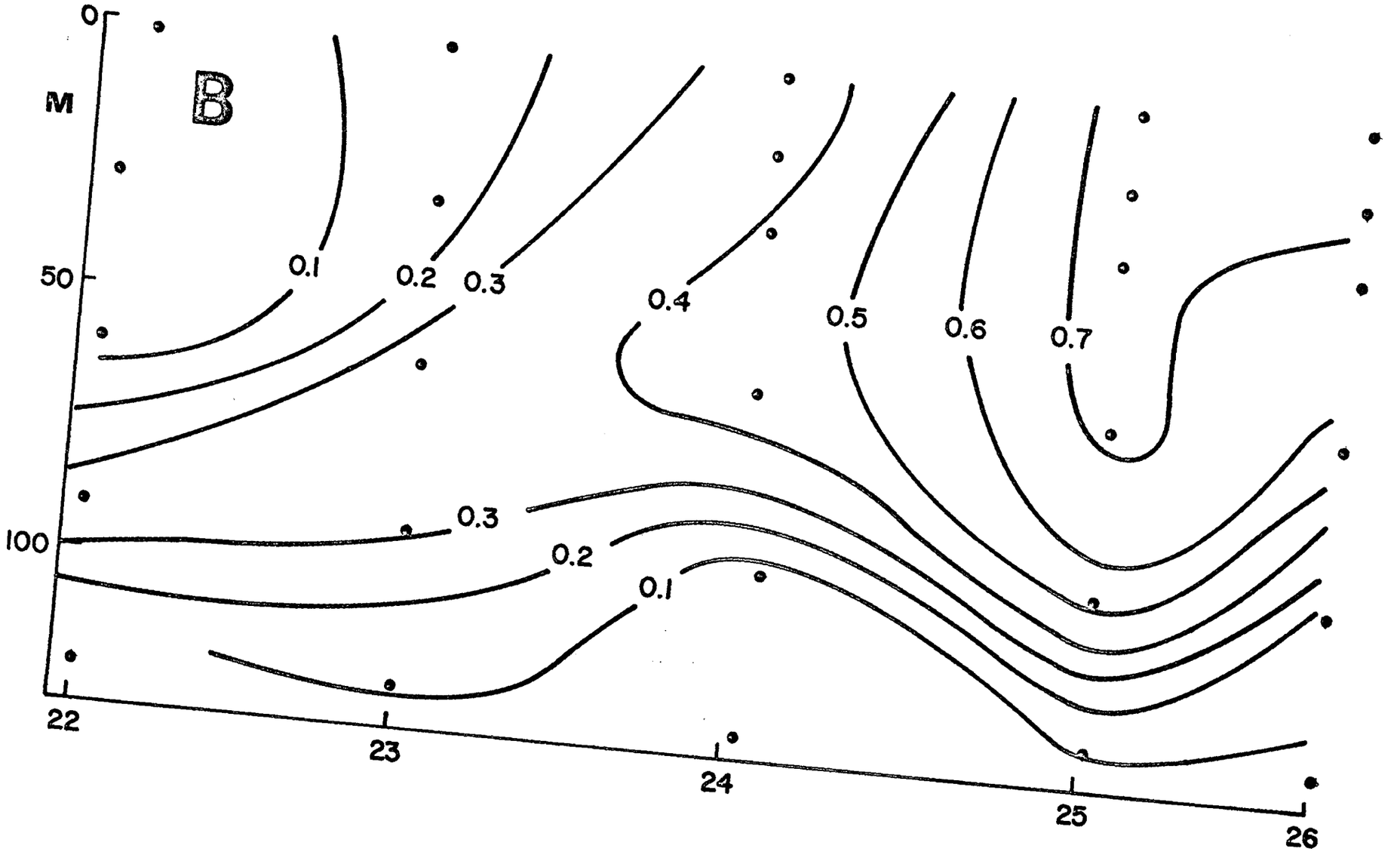

FIGURE 22b

FIGURE 23

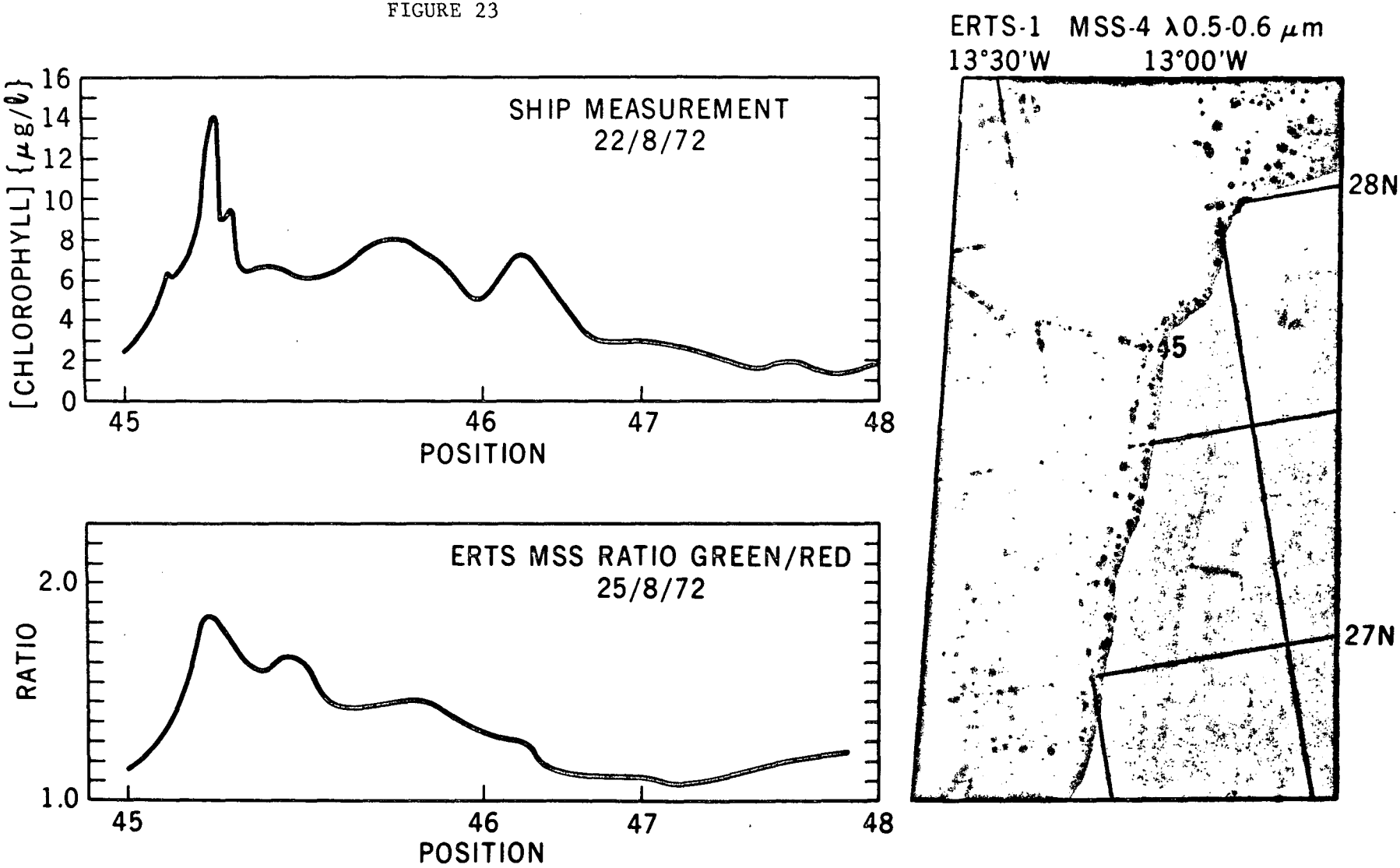
SHIP MEASUREMENT
22/8/72
[CHLOROPHYLL] {μg/ℓ}
16
14
12
10
8
6
4
2
0
45
46
47
48
POSITION
ERTS MSS RATIO GREEN/RED
25/8/72
RATIO
2.0
1.0
45
46
47
48
POSITION
ERTS-1 MSS-4 λ0.5-0.6 μm
13°30'W
13°00'W
28N
45
27N

UPWELLING & PLANKTON PATTERNS
NORTH-WEST AFRICA

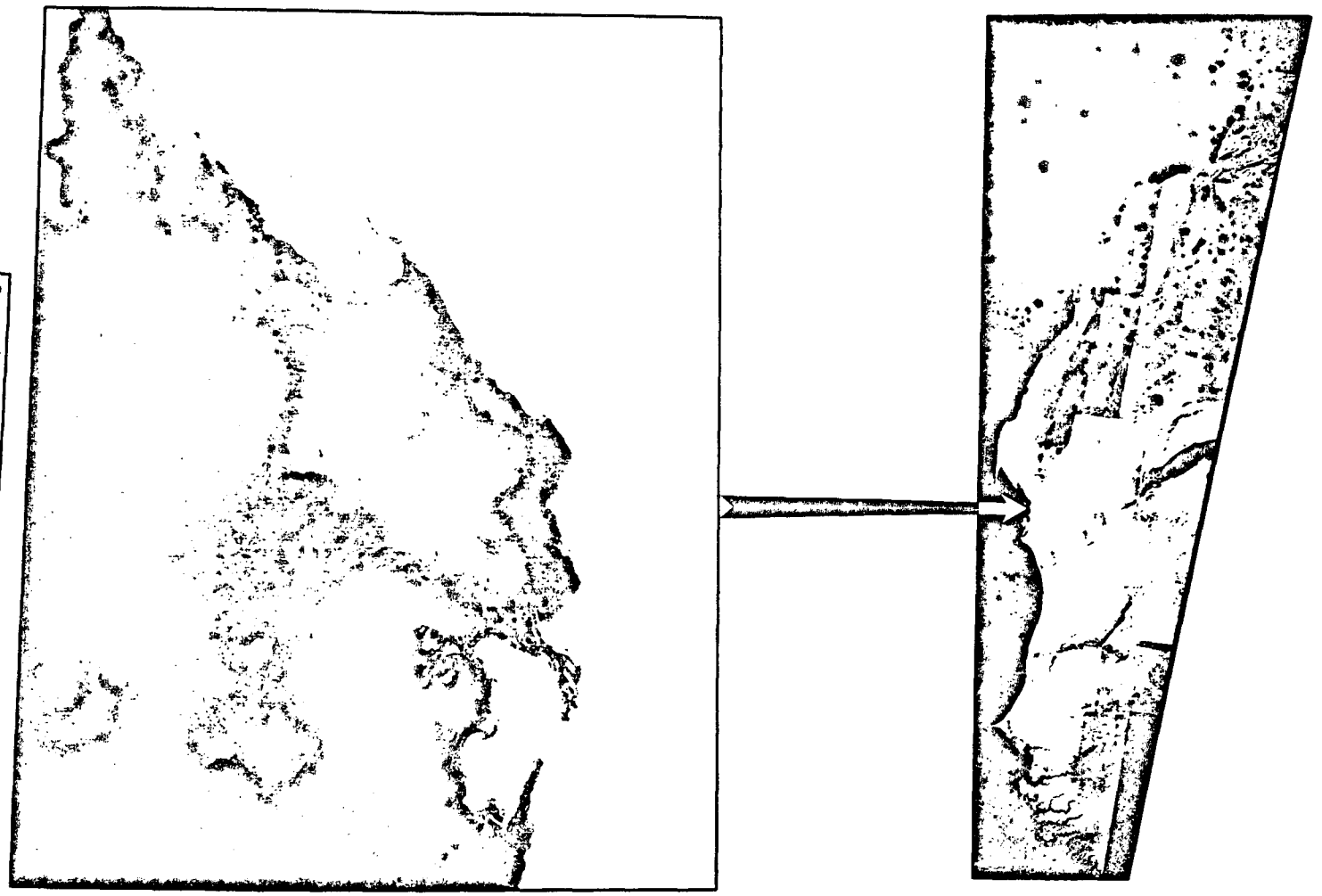

ERTS-1 (GREEN BAND) 22 FEBRUARY 1973

FIGURE 24

GODDARD SPACE FLIGHT CENTER
GREENBELT, MARYLAND

73.9696

UPWELLING & PLANKTON PATTERNS
NORTH-WEST AFRICA

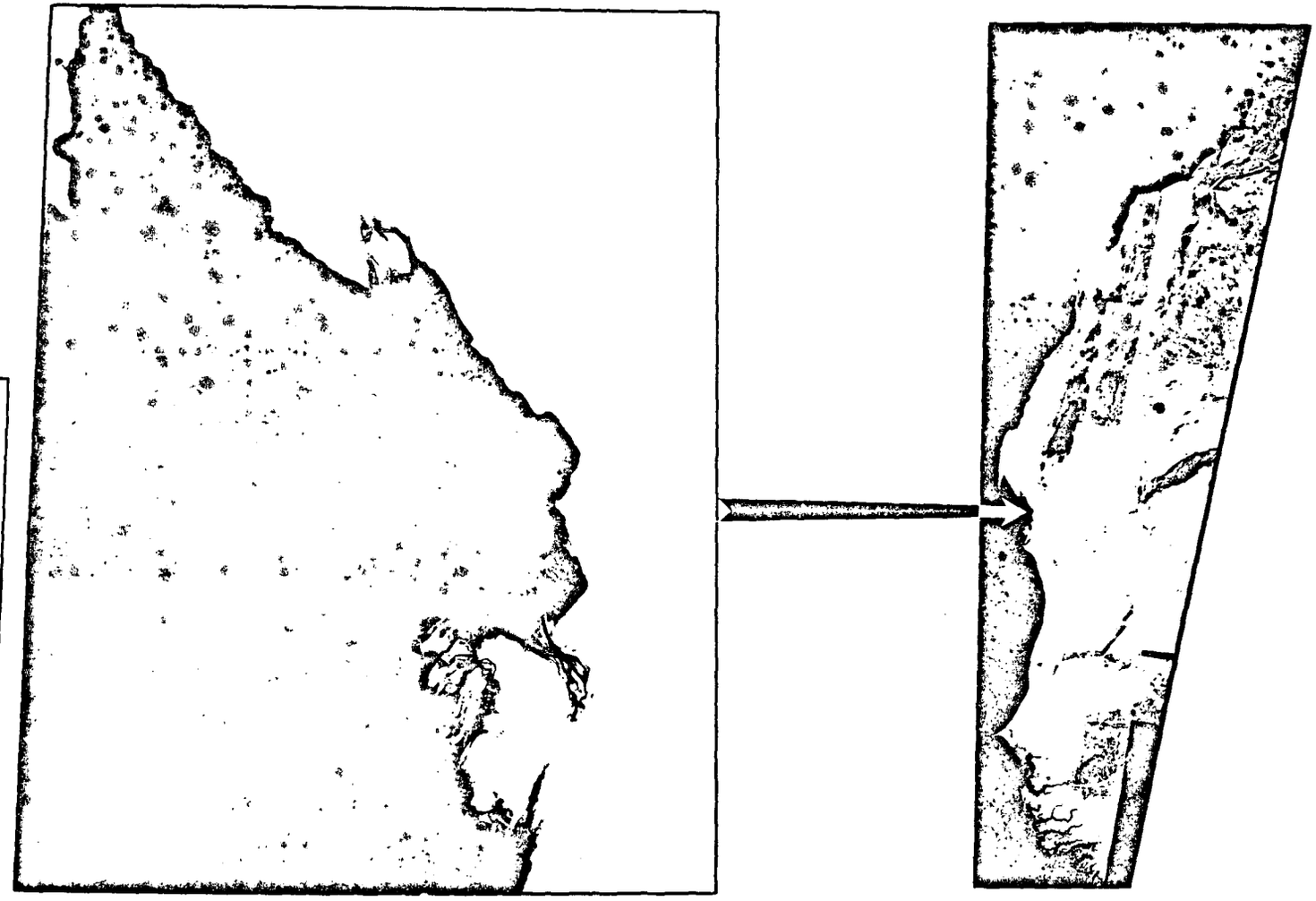

ERTS-1 (RED BAND) 22 FEBRUARY 1973

FIGURE 25

GODDARD SPACE FLIGHT CENTER
GREENBELT, MARYLAND
73-9699

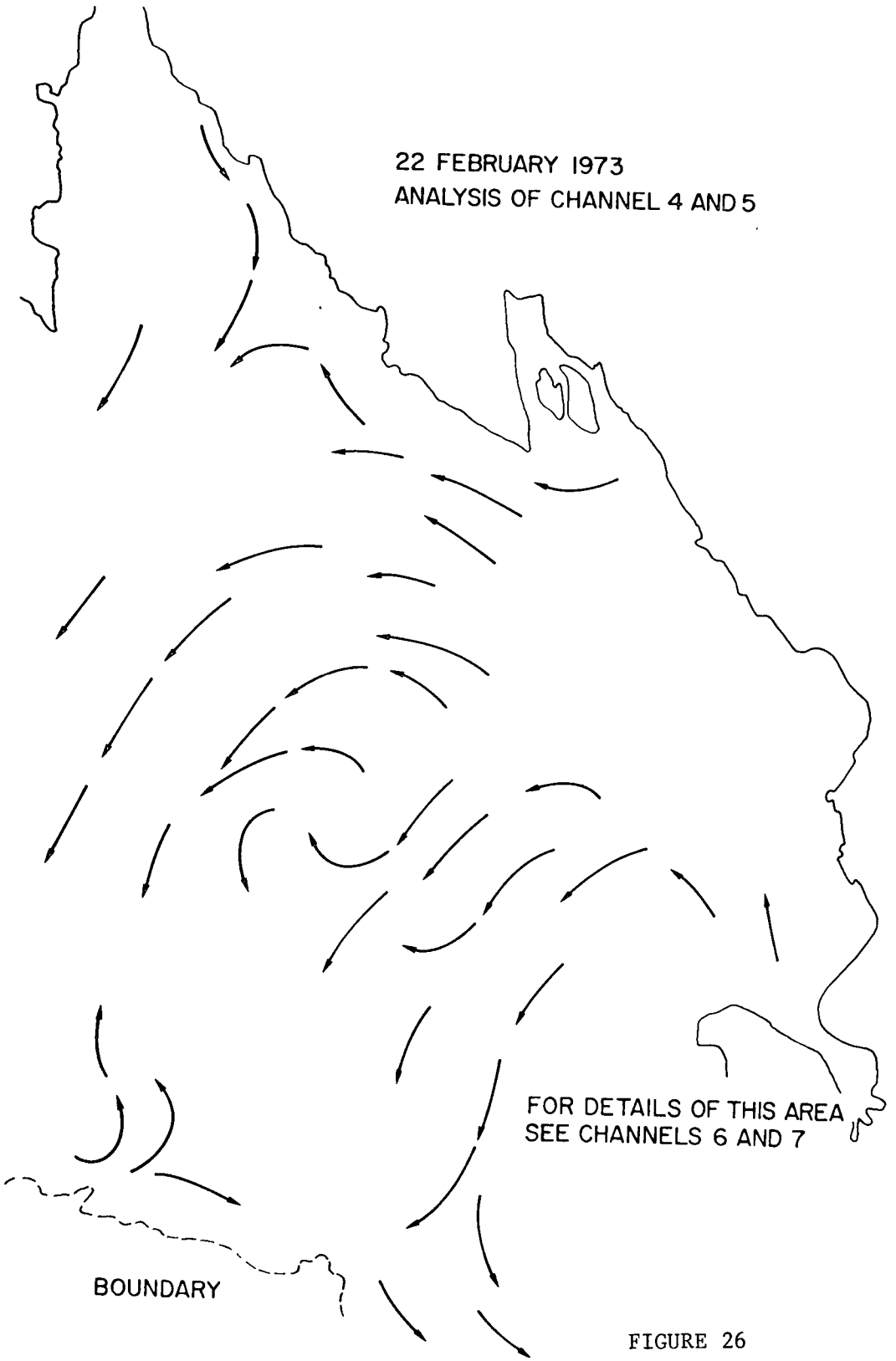
22 FEBRUARY 1973
ANALYSIS OF CHANNEL 4 AND 5
FOR DETAILS OF THIS AREA
SEE CHANNELS 6 AND 7
BOUNDARY

FIGURE 26

Figure 27

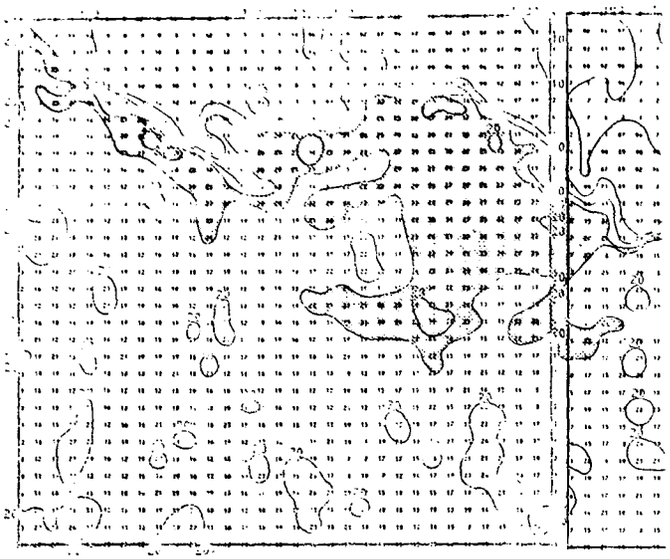

REFLECTED ENERGY

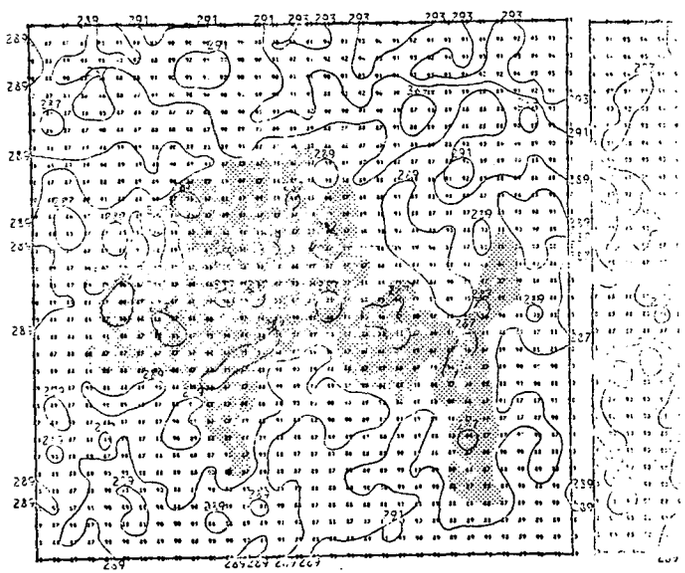

INFRARED RECORDINGS

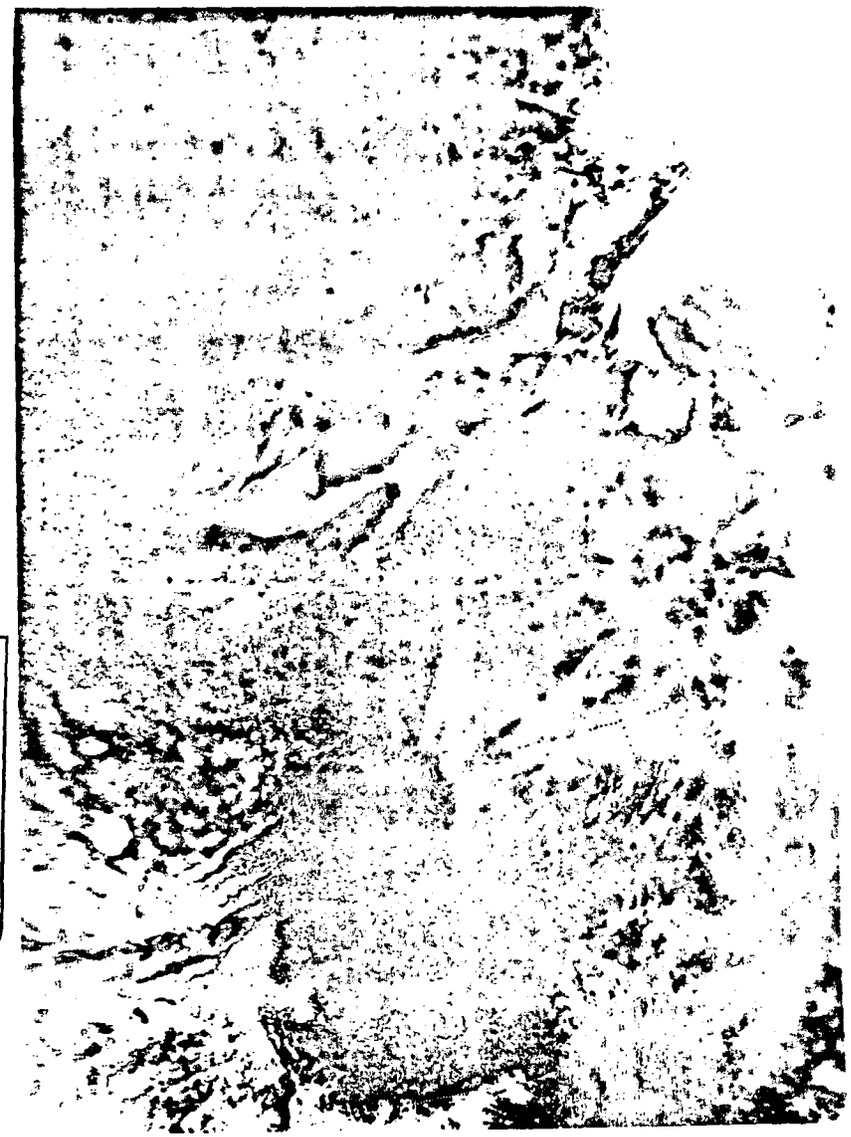

OBSERVATIONS WITH NOAA 2 ON 22 FEBRUARY 1973